(Journal of Climate)

Estimates of Meridional Atmosphere and Ocean Heat Transports

KEVIN E. TRENBERTH AND JULIE M. CARON

National Center for Atmospheric Research, Boulder, Colorado*

(Manuscript received 8 November 2000, in final form 21 February 2001)

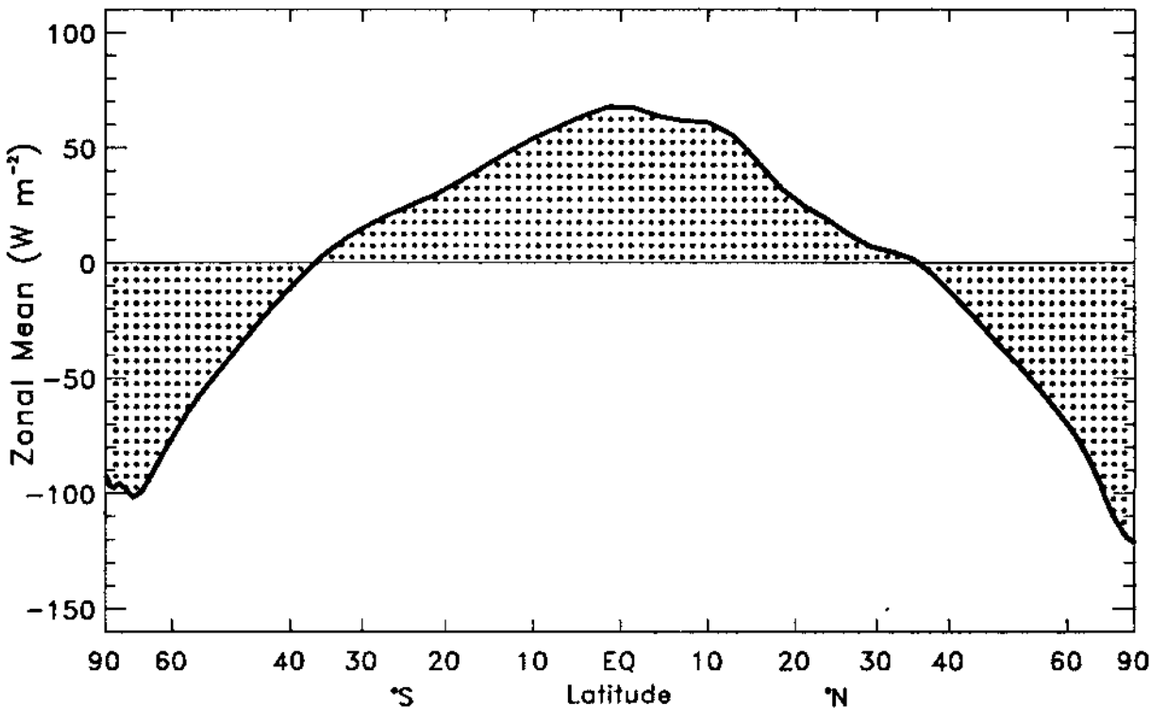

FIG. 1. TOA annualized ERBE zonal mean net radiation (W m^{-2}) for Feb 1985–Apr 1989.

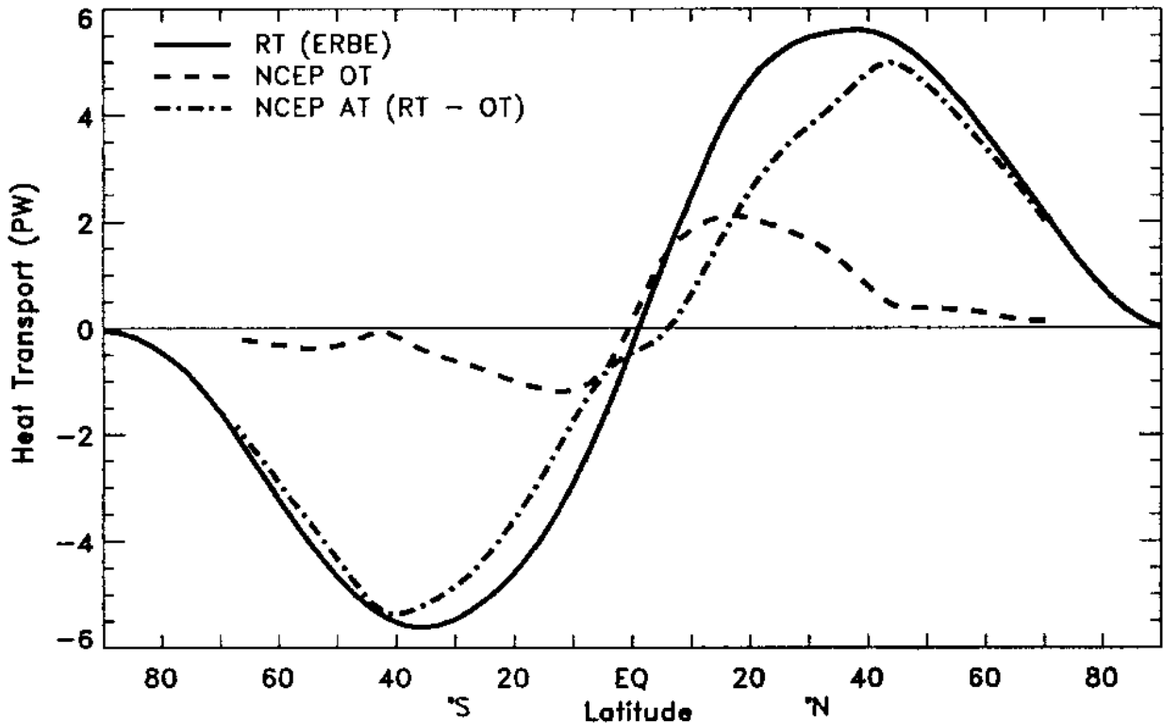

FIG. 7. The required total heat transport from the TOA radiation RT is compared with the derived estimate of the adjusted ocean heat transport OT (dashed) and implied atmospheric transport AT from NCEP reanalyses (PW).

Time-averaged (16-year) ocean circulation

Wunsch, 2011

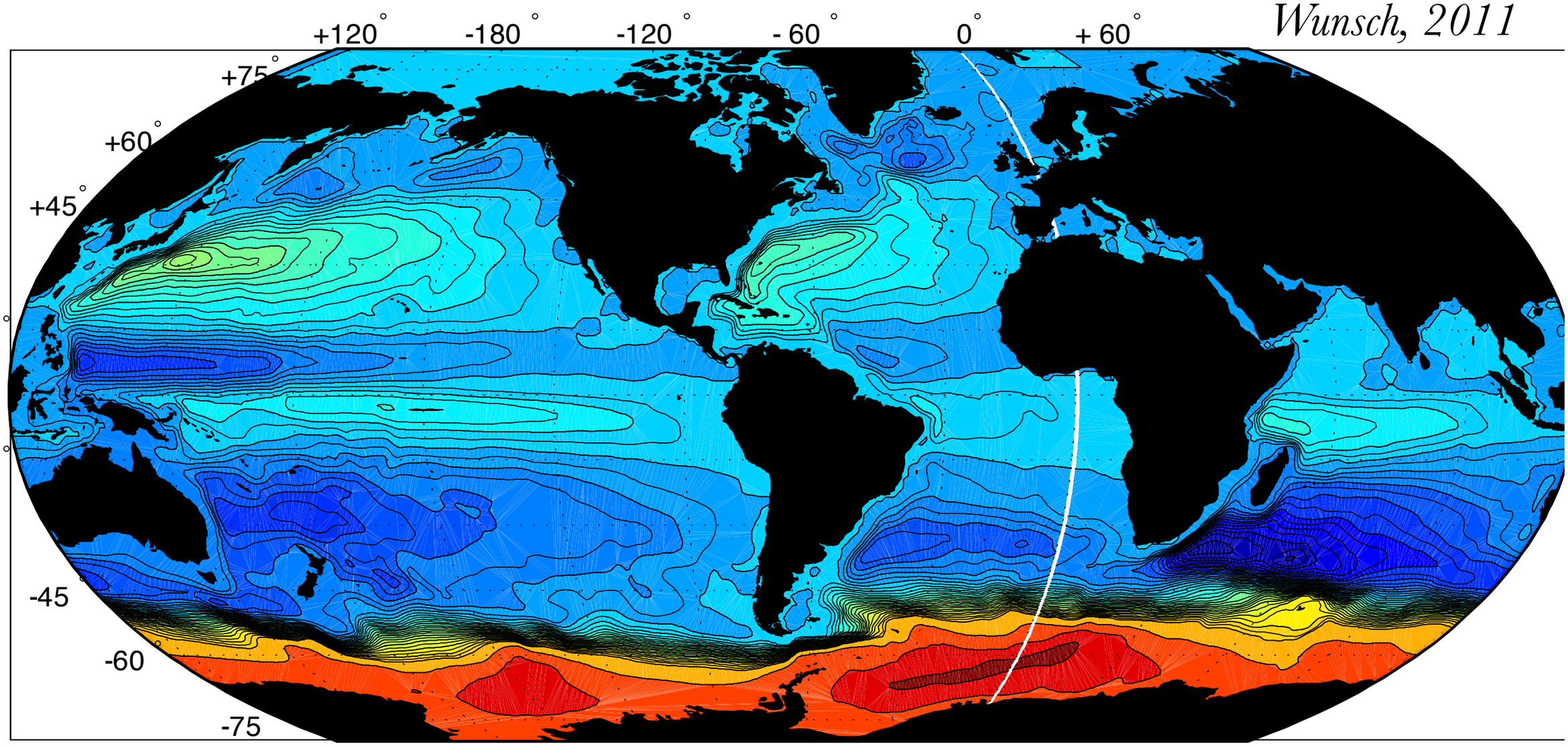

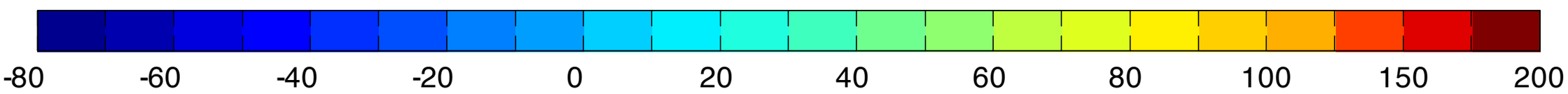

Transport streamfunction (10^6 m^3/s = 1 Sverdrup)

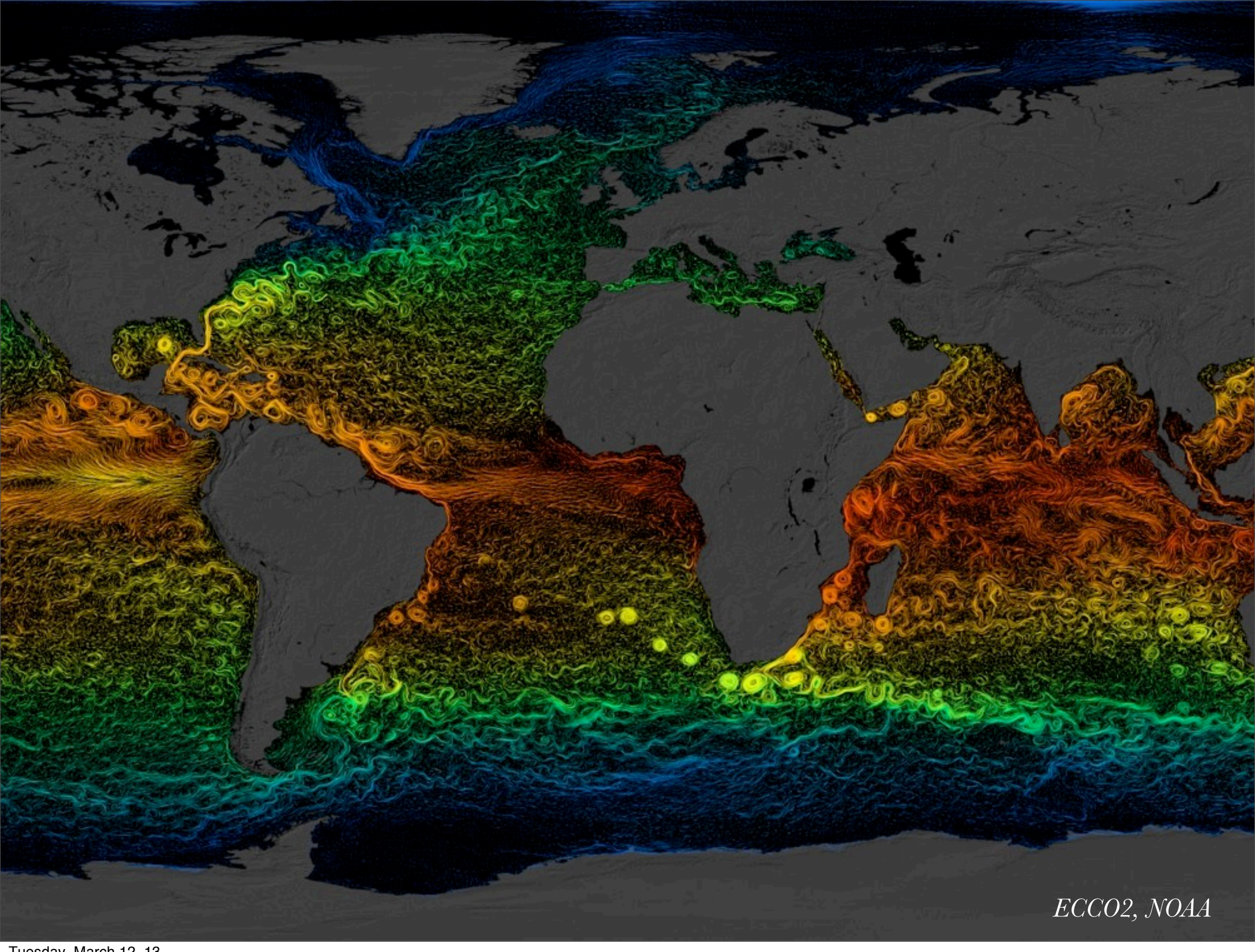
ECCO2, NOAA

LONG-TERM GLOBAL WARMING SCENARIOS COMPUTED WITH AN EFFICIENT COUPLED CLIMATE MODEL

STEFAN RAHMSTORF and ANDREY GANOPOLSKI
Potsdam Institute for Climate Research, Telegrafenberg, 14472 Potsdam, Germany

Climatic Change **43:** 353–367, 1999.
© 1999 *Kluwer Academic Publishers. Printed in the Netherlands.*

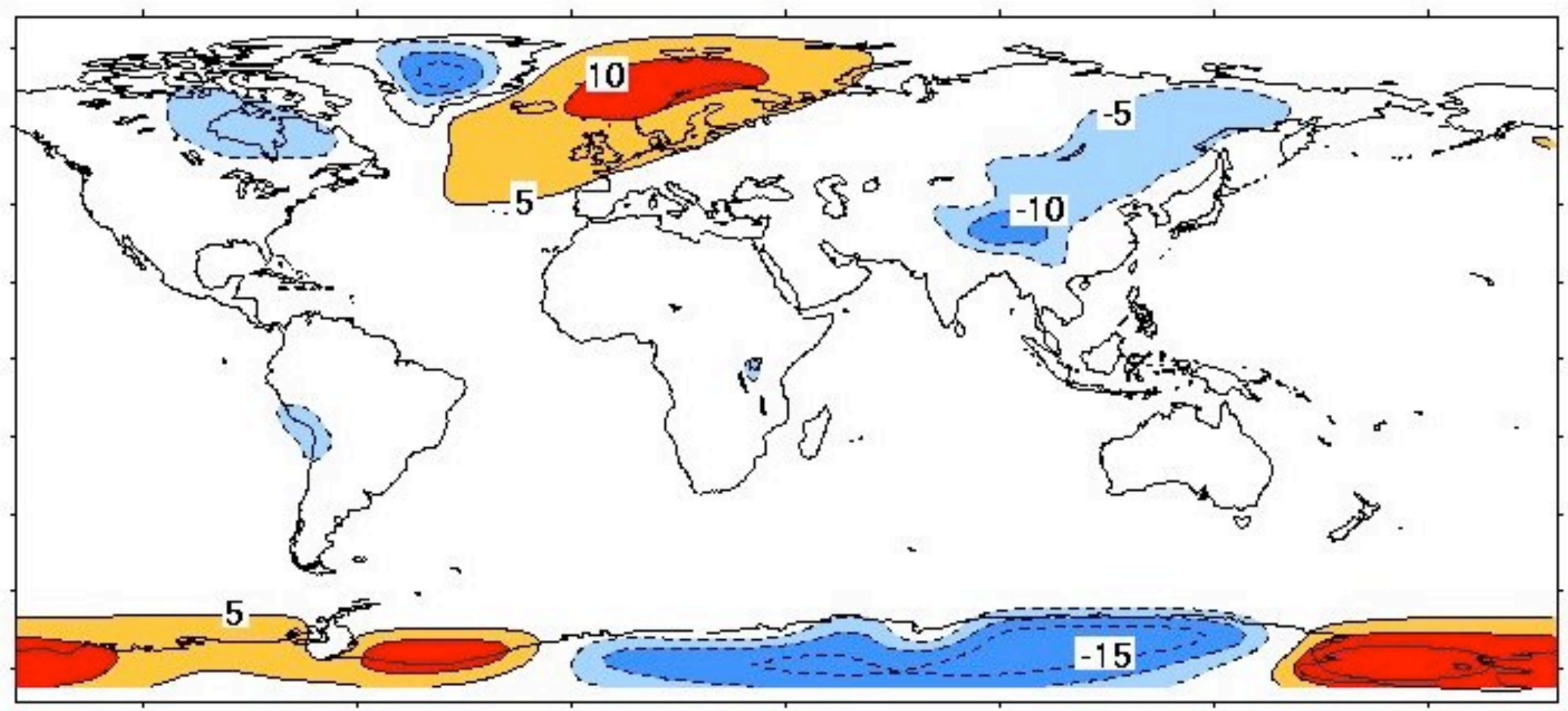

Figure 1. Deviation of the annual-mean surface air temperature from its zonal average, computed from the NCAR air temperature climatology. Anomalously cold areas are found over some continental regions, anomalously warm areas over ocean deep water formation regions.

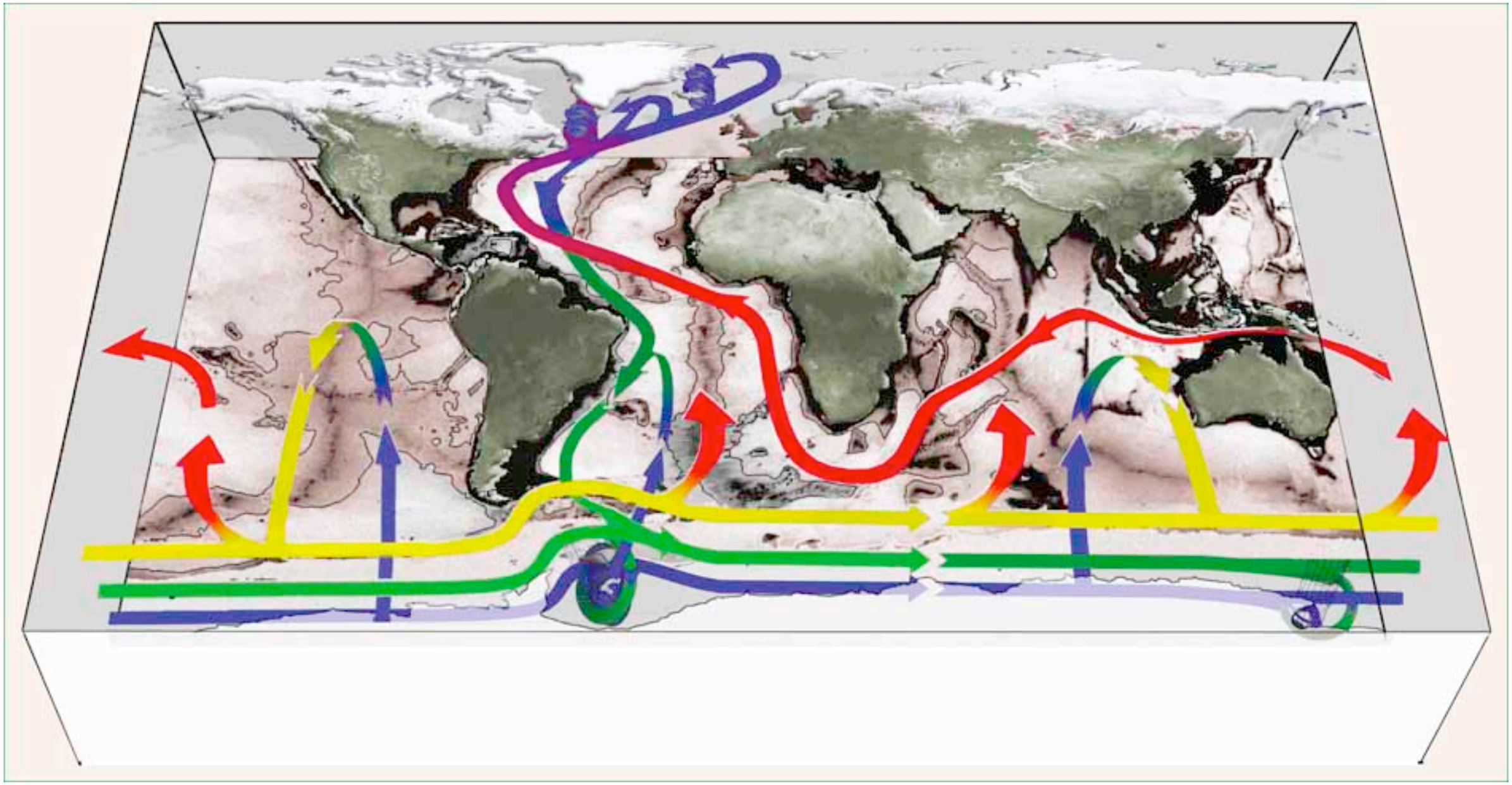

Closure of the meridional overturning circulation through Southern Ocean upwelling

John Marshall[1]* and Kevin Speer[2]

Overturning Circulation

Averaging, across an ocean in longitude

- Meridional Overturning Circulation (MOC)
  (sometimes called the Thermohaline Circulation, THC)

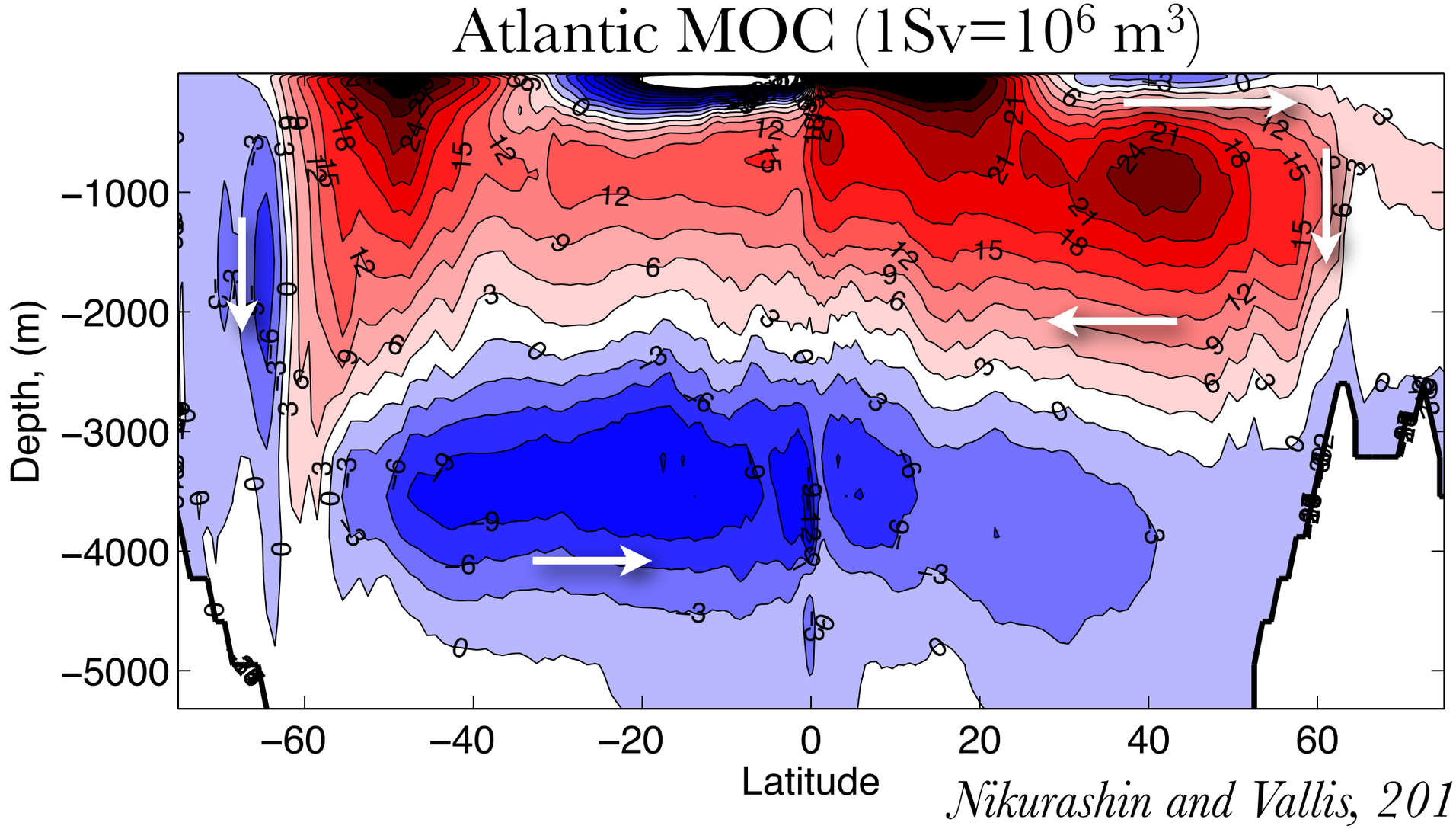

Nikurashin and Vallis, 2011

Rahmstorf, Nature 2002

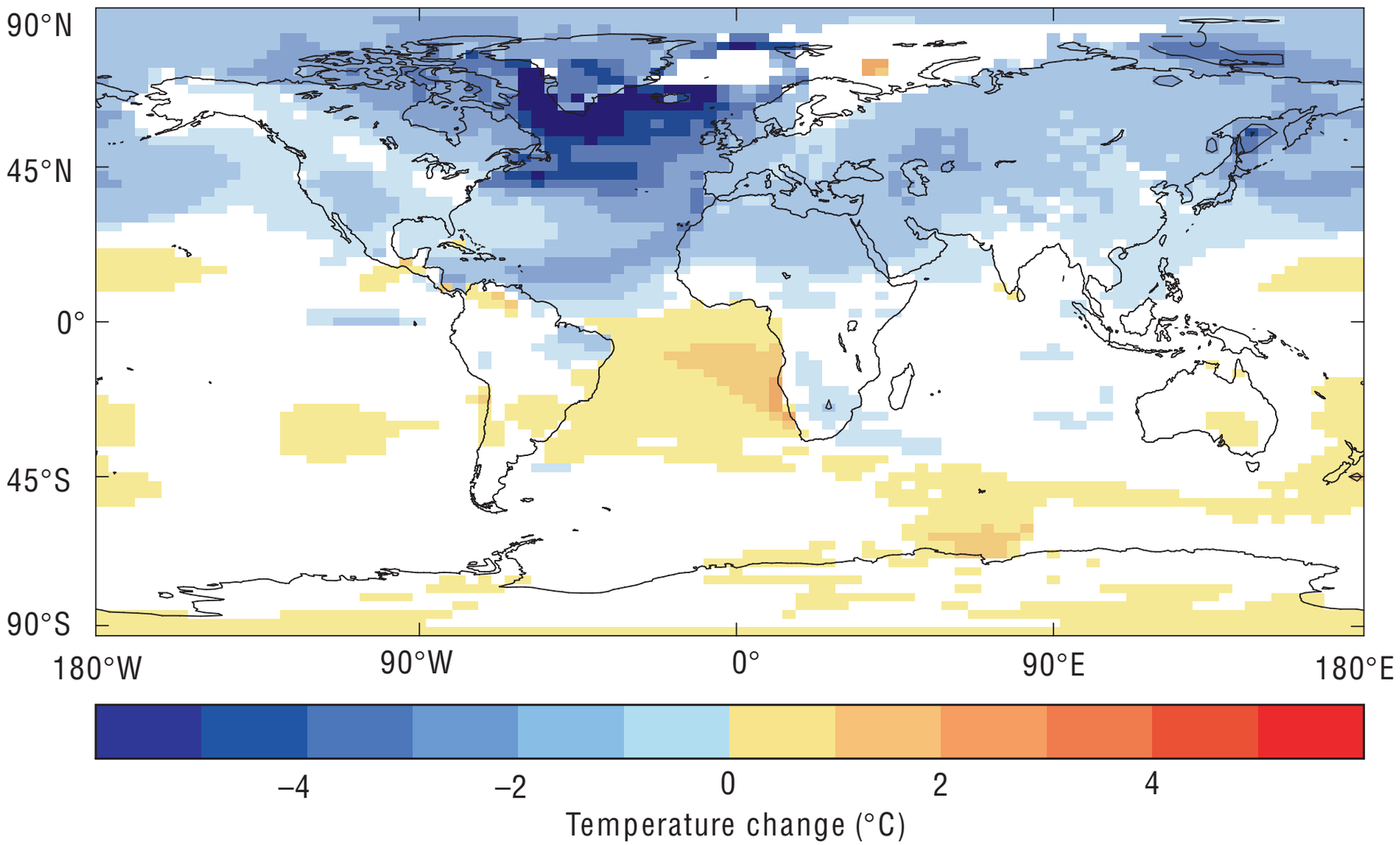

Figure 1 Changes in surface air temperature caused by a shutdown of North Atlantic Deep Water (NADW) formation in a current ocean–atmosphere circulation model. Note the hemispheric see-saw (Northern Hemisphere cools while the Southern Hemisphere warms) and the maximum cooling over the northern Atlantic. In this particular model (HadCM3)[7], the surface cooling resulting from switching off NADW formation is up to 6 °C. It is further to the west compared with most models, which tend to put the maximum cooling near Scandinavia. This probably depends on the exact location of deep-water formation (an aspect not well represented in current coarse-resolution models) and on the sea-ice distribution in the models, as ice-margin shifts act to amplify the cooling. The largest air temperature cooling is thus greater than the largest sea surface temperature (SST) cooling. The latter is typically around 5 °C and roughly corresponds to the observed SST difference between the northern Atlantic and Pacific at a given latitude. In most models, maximum air temperature cooling ranges from 6 °C to 11 °C in annual mean; the effect is generally stronger in winter.

Rahmstorf, Nature 2002

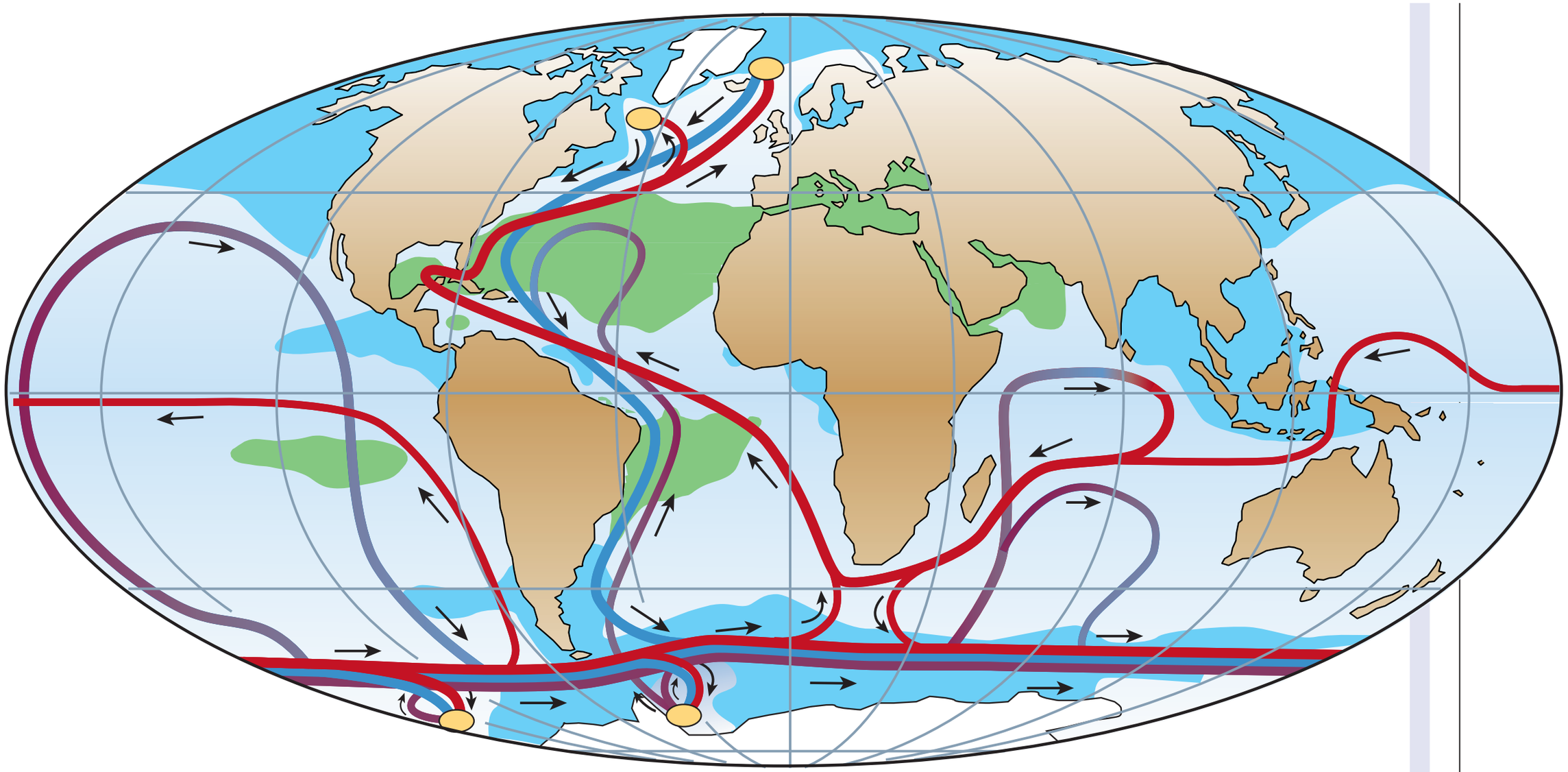

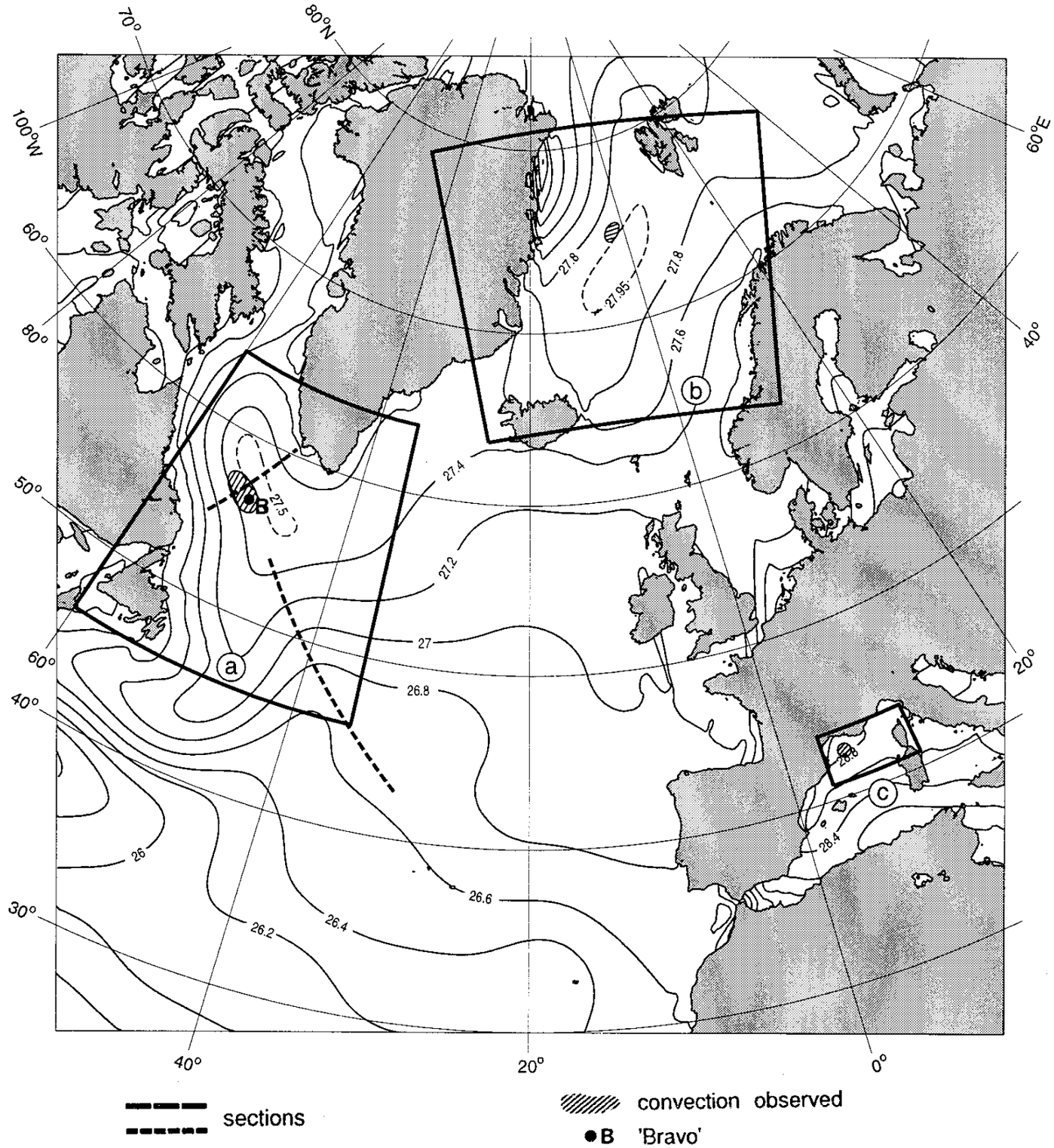

Figure 1. The major deep convection sites of the North Atlantic sector: the Labrador Sea (box a), the Greenland Sea (box b), and the western Mediterranean (box c). Detailed descriptions and discussions of the water mass transformation process occurring in the three "boxes" are reviewed here. To indicate the preconditioned state of early winter, the potential density at a depth of 100 m is shown for November from the climatological data of *Levitus et al*. [1994b] and *Levitus and Boyer* [1994]. Deep-reaching convection has been observed in the shaded regions.

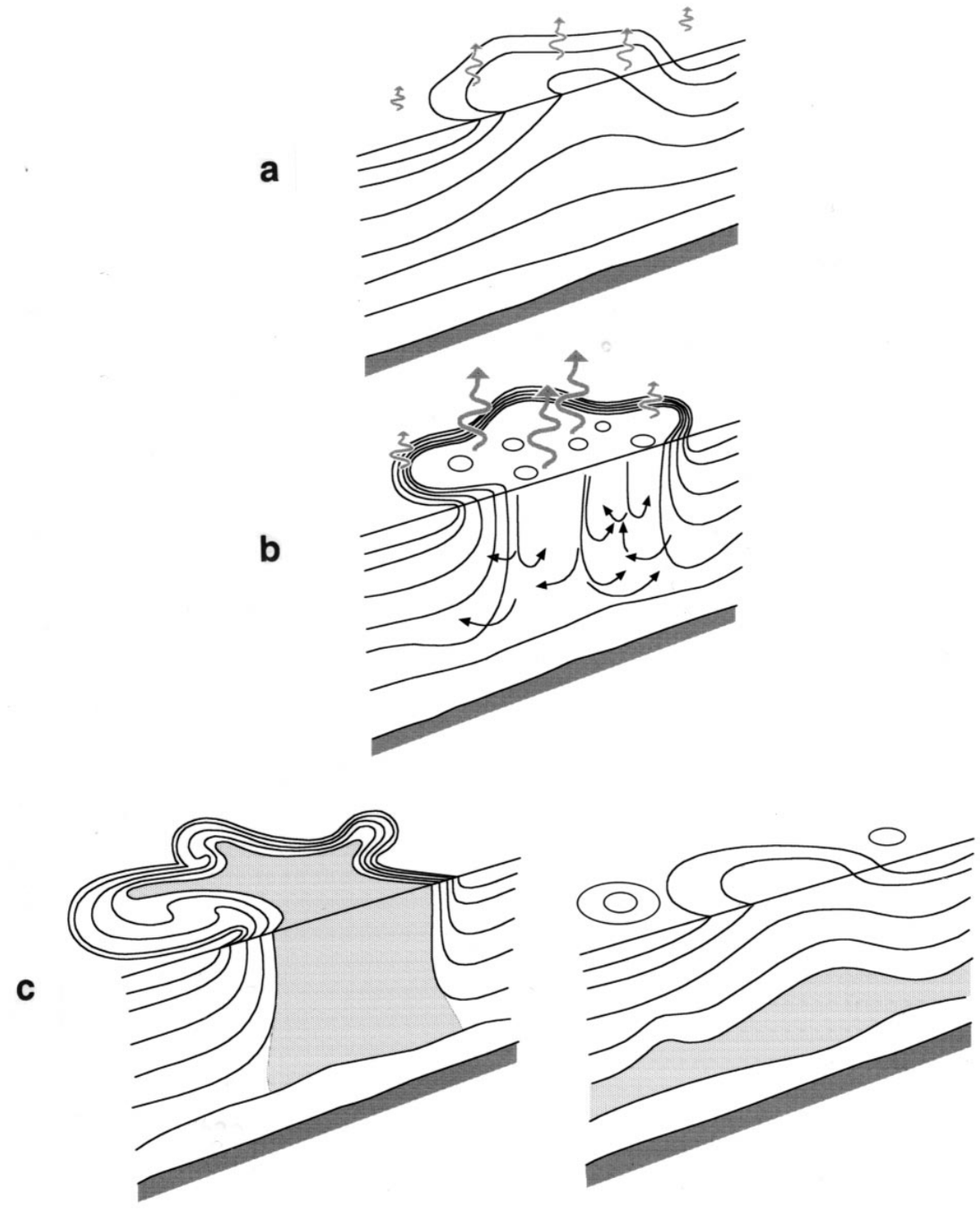

Figure 3. Schematic diagram of the three phases of open-ocean deep convection: (a) preconditioning, (b) deep convection, and (c) lateral exchange and spreading. Buoyancy flux through the sea surface is represented by curly arrows, and the underlying stratification/outcrops is shown by continuous lines. The volume of fluid mixed by convection is shaded.

eWOCE

Potential Temperature θ [°C]

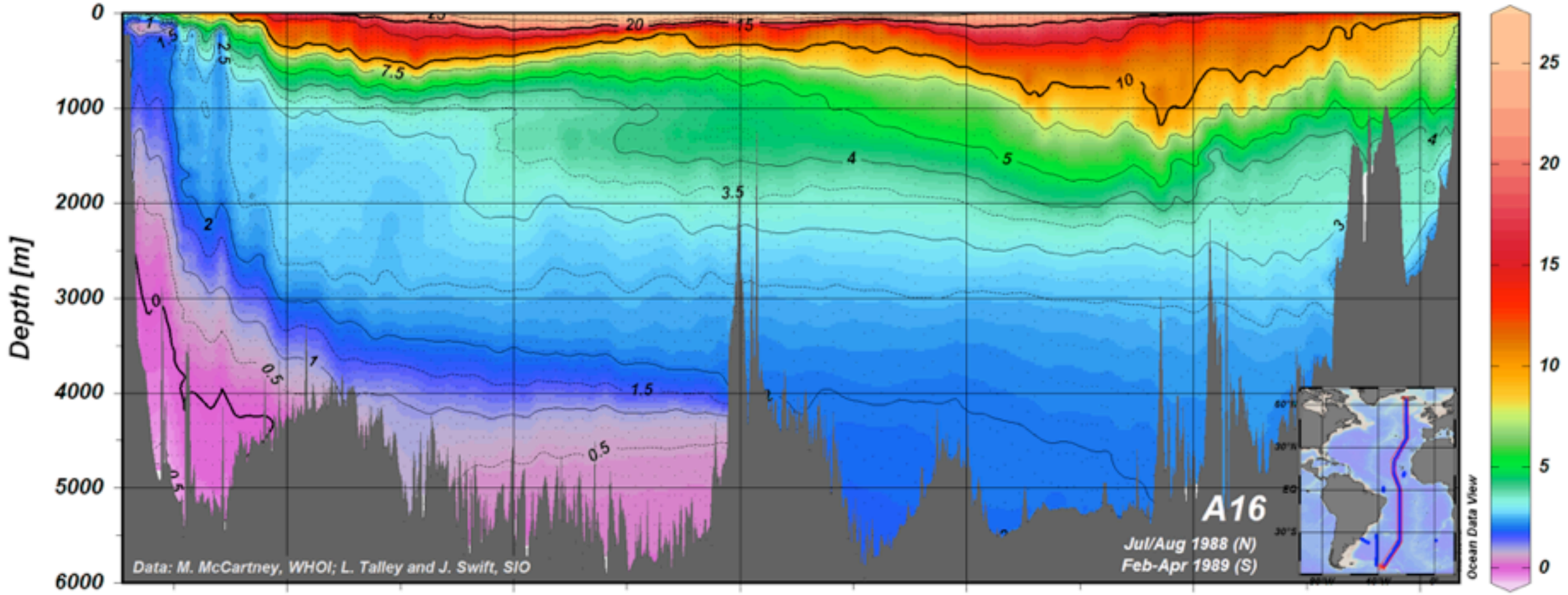

Salinity [pss-78]

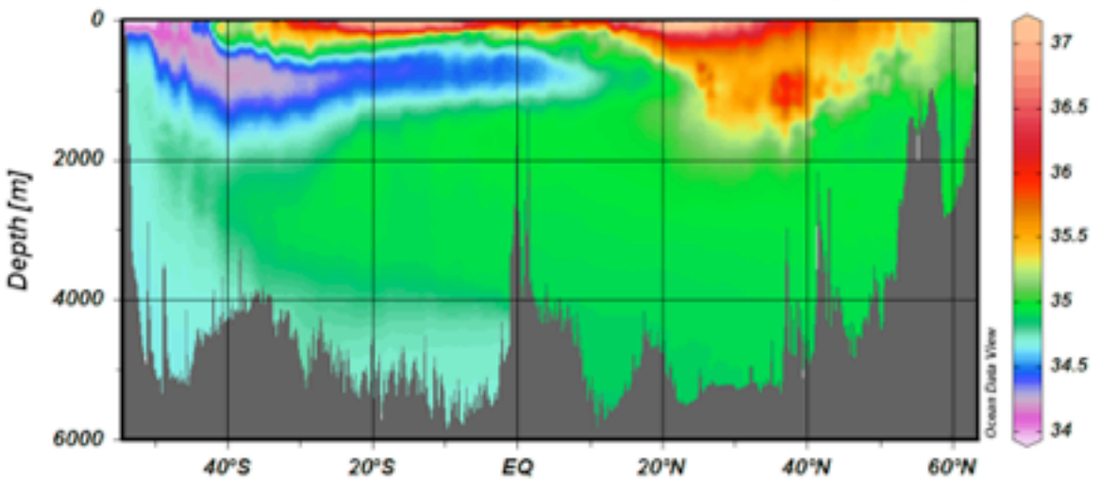

Silicate [µmol/kg]

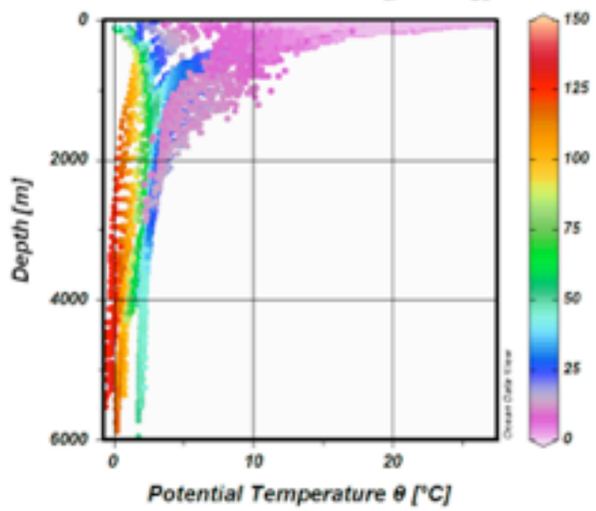

Silicate [µmol/kg]

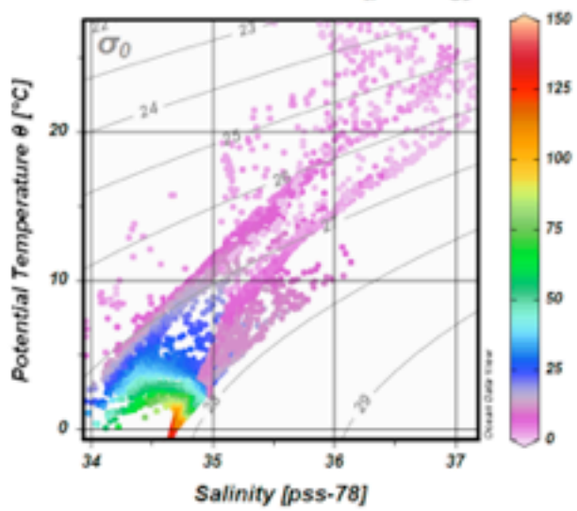

eWOCE

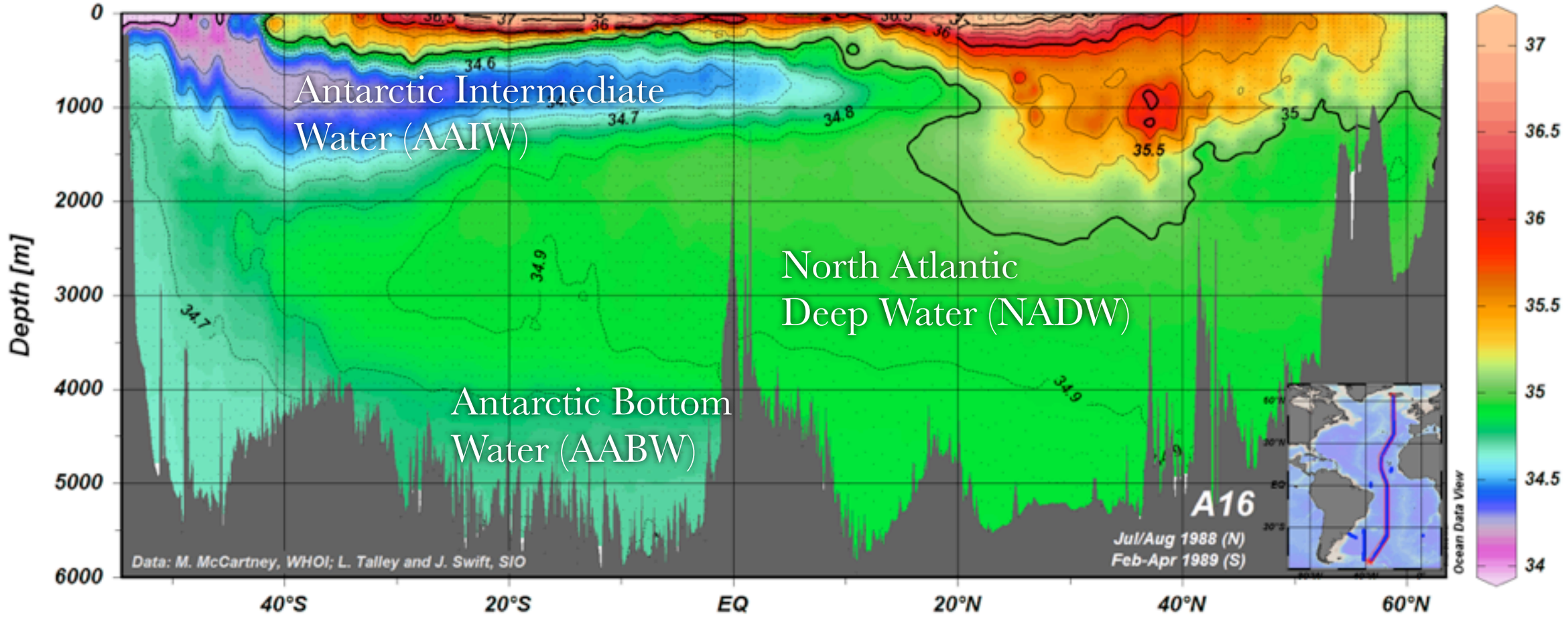
Salinity [pss-78]
Antarctic Intermediate Water (AAIW)
North Atlantic Deep Water (NADW)
Antarctic Bottom Water (AABW)
A16
Jul/Aug 1988 (N)
Feb-Apr 1989 (S)
Data: M. McCartney, WHOI; L. Talley and J. Swift, SIO
Depth [m]
40°S
20°S
EQ
20°N
40°N
60°N
Ocean Data View

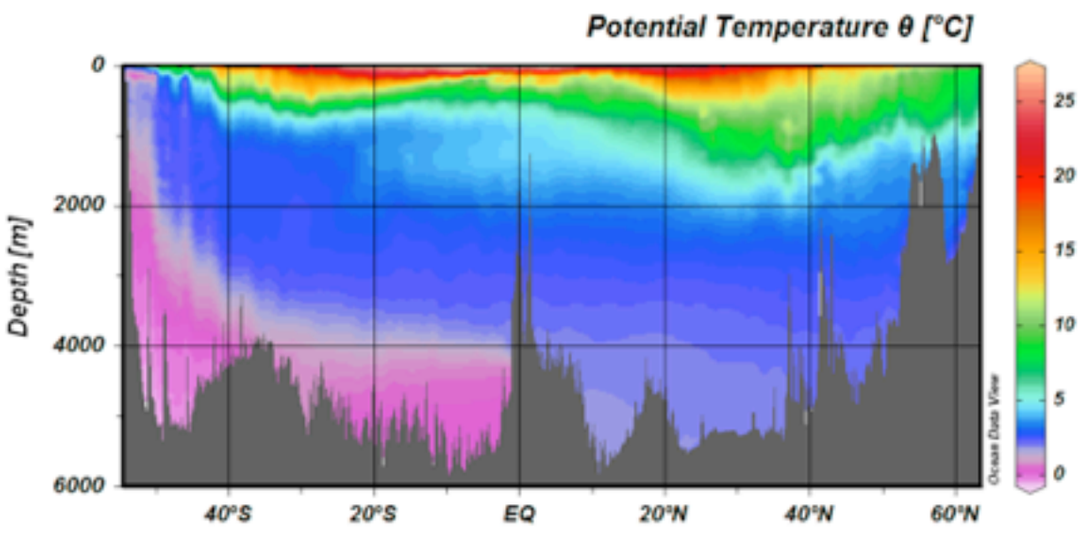
Potential Temperature θ [°C]
Depth [m]
Ocean Data View

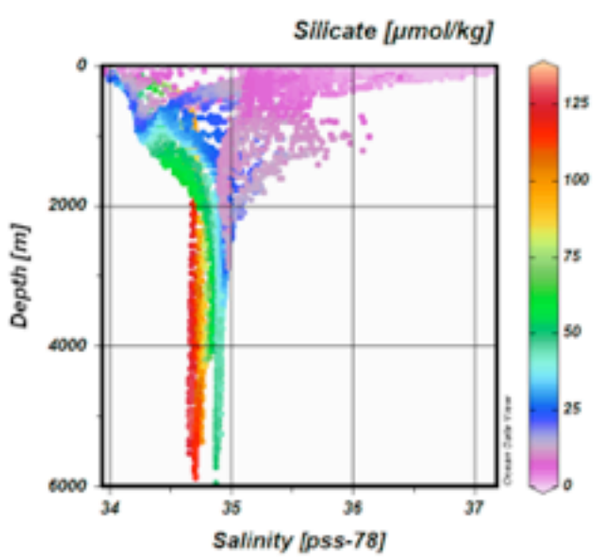
Silicate [µmol/kg]
Depth [m]
Salinity [pss-78]
Ocean Data View

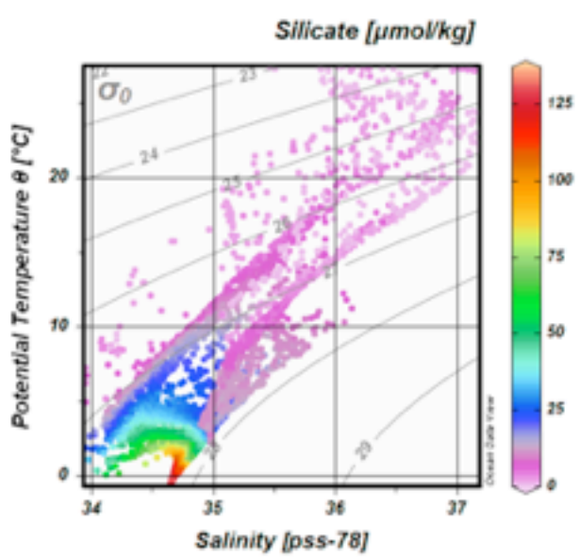
Silicate [µmol/kg]
Potential Temperature θ [°C]
Salinity [pss-78]
Ocean Data View

eWOCE

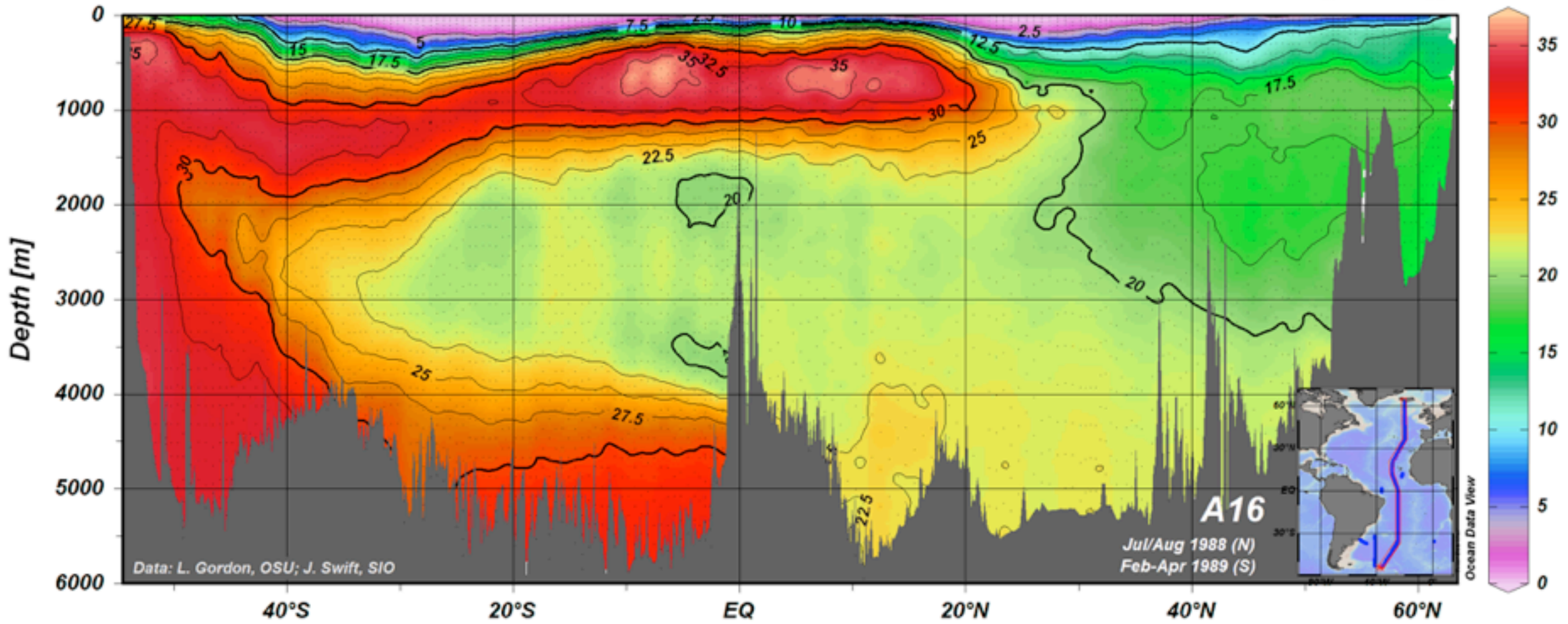
Nitrate [µmol/kg]
Depth [m]
0
1000
2000
3000
4000
5000
6000
40°S
20°S
EQ
20°N
40°N
60°N
Data: L. Gordon, OSU; J. Swift, SIO
A16
Jul/Aug 1988 (N)
Feb-Apr 1989 (S)
Ocean Data View
35
30
25
20
15
10
5
0

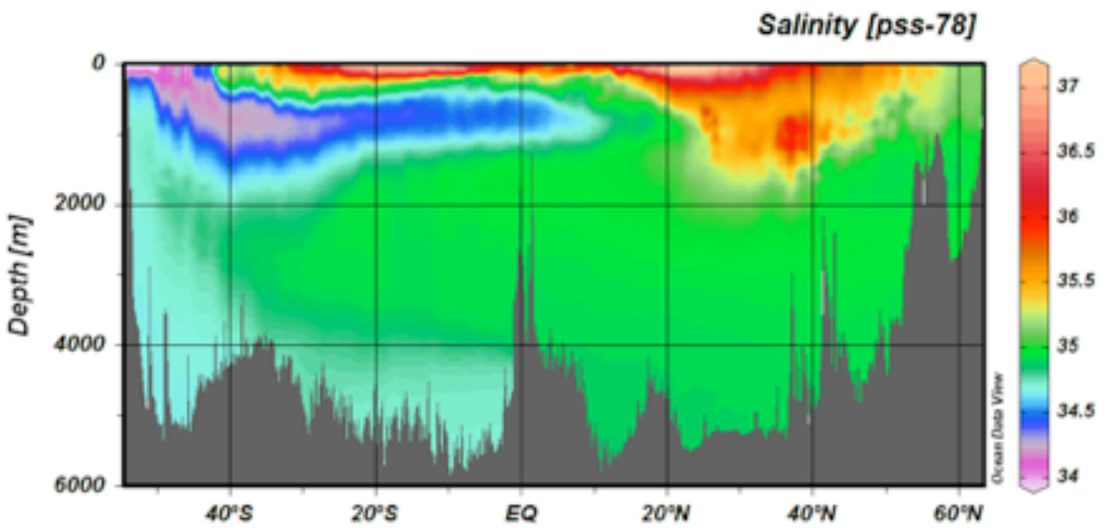
Salinity [pss-78]
Depth [m]
0
2000
4000
6000
40°S
20°S
EQ
20°N
40°N
60°N
37
36.5
36
35.5
35
34.5
34

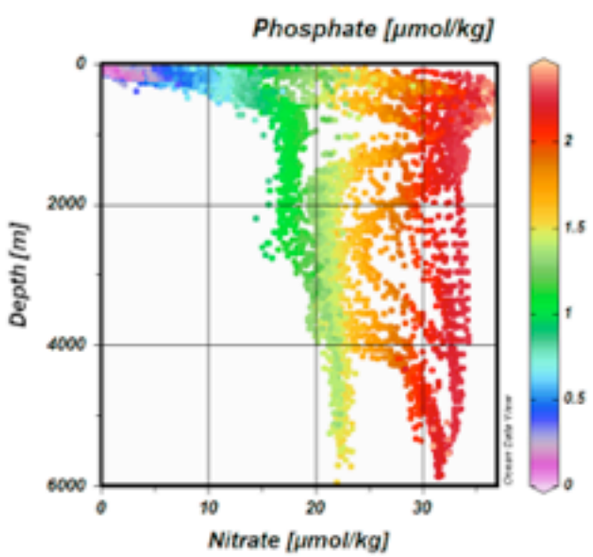
Phosphate [µmol/kg]
Depth [m]
0
2000
4000
6000
0
10
20
30
Nitrate [µmol/kg]
2
1.5
1
0.5
0

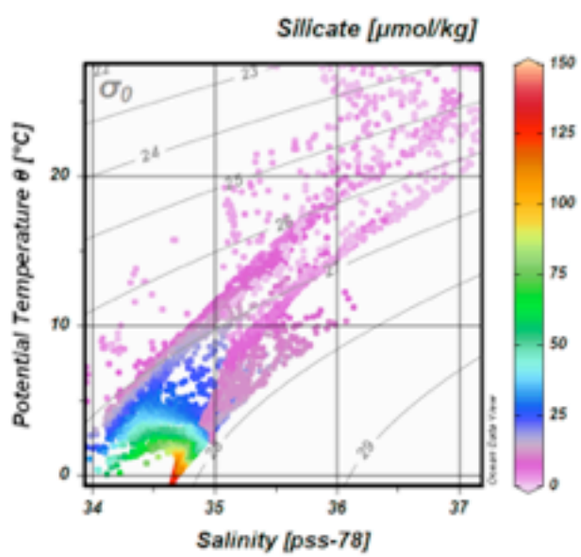
Silicate [µmol/kg]
Potential Temperature θ [°C]
20
10
0
34
35
36
37
Salinity [pss-78]
150
125
100
75
50
25
0

Vertical Density Structure

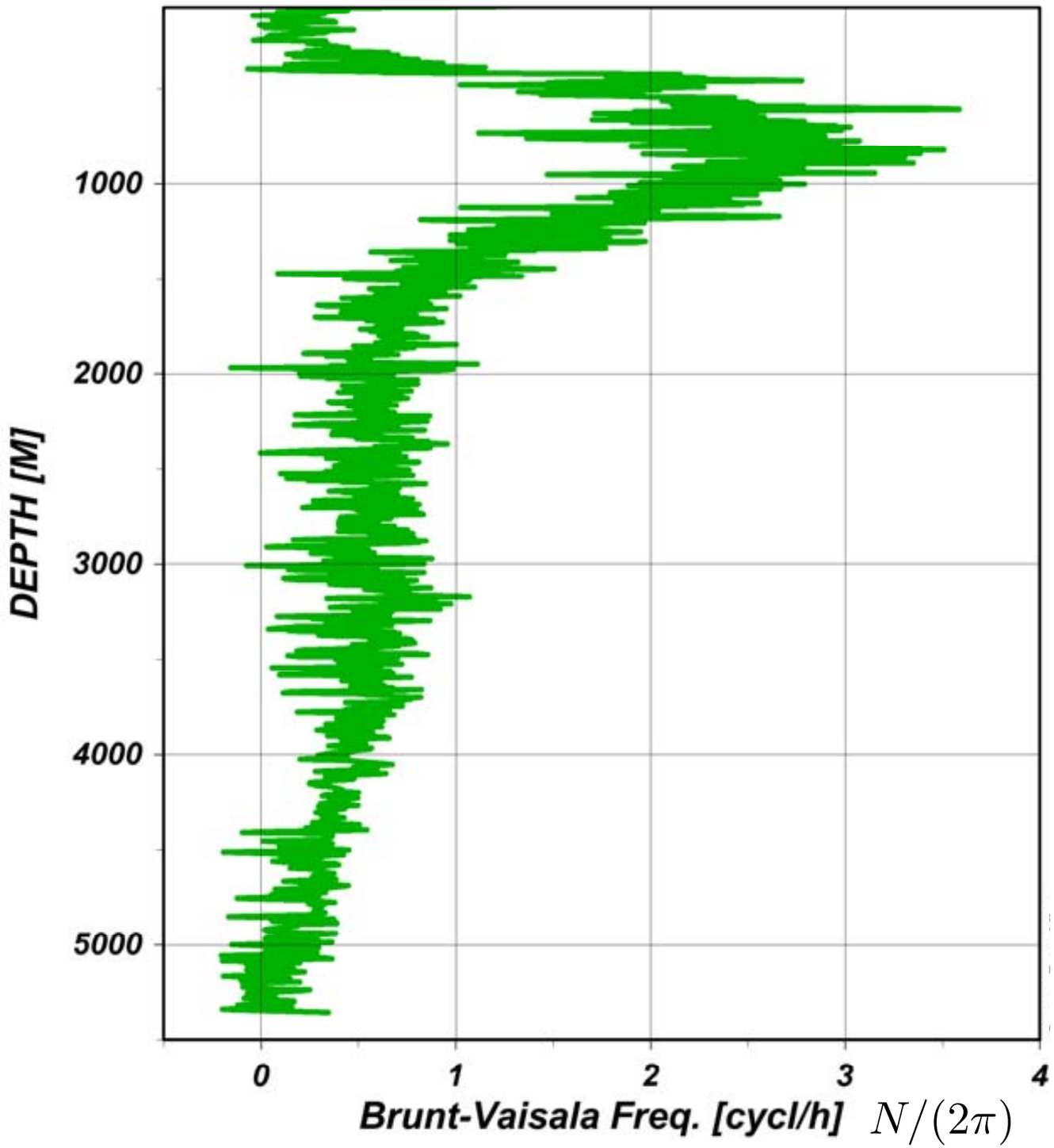

Mixed layer

Thermocline

Abyss

$N/(2\pi)$

$$N^2 = -\frac{g}{\rho_0}\frac{\partial \rho}{\partial z}$$

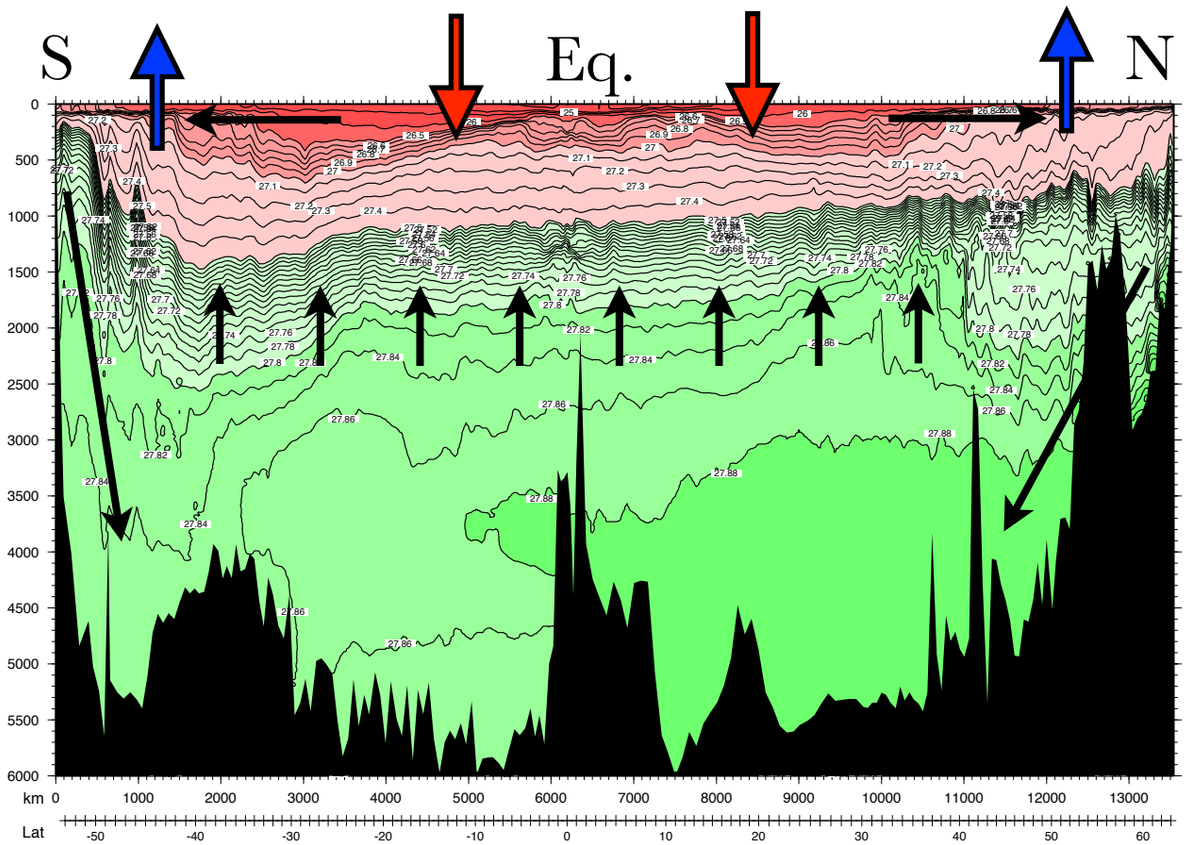

Deep-Sea Research, 1966, Vol. 13, pp. 707 to 730. Pergamon Press Ltd. Printed in Great Britain.

Abyssal recipes

WALTER H. MUNK*

(*Received* 31 *January* 1966)

Without a means to transport heat down from the surface, the sinking of dense water at the poles would eventually fill the ocean with cold water.

1D (horizontally-averaged) density equation:

$$\frac{\partial \overline{\rho}}{\partial t} + \overline{w}\frac{\partial \overline{\rho}}{\partial z} + \frac{\partial}{\partial z}\overline{w'\rho'} = \kappa \frac{\partial^2 \overline{\rho}}{\partial z^2}$$

Define the *turbulent* diffusivity $\kappa_T \equiv \dfrac{-\overline{w'\rho'}}{\partial \overline{\rho}/\partial z}$

$$\frac{\partial \overline{\rho}}{\partial t} + \overline{w}\frac{\partial \overline{\rho}}{\partial z} = \frac{\partial}{\partial z}\left((\kappa + \kappa_T)\frac{\partial \overline{\rho}}{\partial z}\right)$$

At steady state, neglecting molecular diffusion and *assuming* $\kappa_T = \text{const.}$

$$\overline{w}\frac{\partial \overline{\rho}}{\partial z} = \kappa_T \frac{\partial^2 \overline{\rho}}{\partial z^2}$$

Munk 1966 *inferred* κ_T using $\overline{\rho}(z),$ and $\overline{w}$

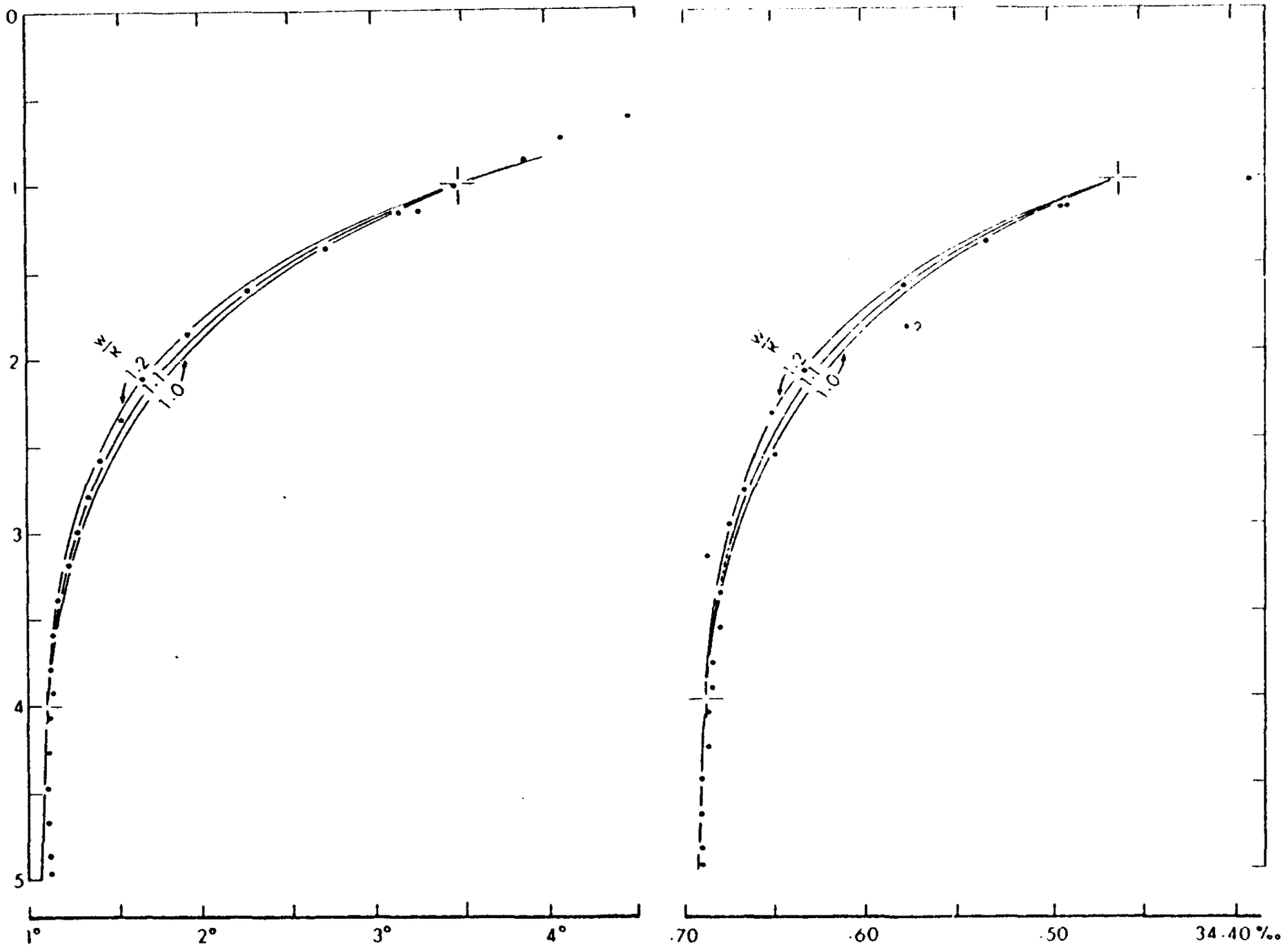

Fig. 3. Potential temperature and salinity as functions of depth (km) at station *Calcofi* 1964: # 60·190, 33° 17′N, 132° 42·5′W (salinity at depth 1859 m was questioned in the original observations). Curves labeled w/κ (in units km^{-1}) are based on equation (1).

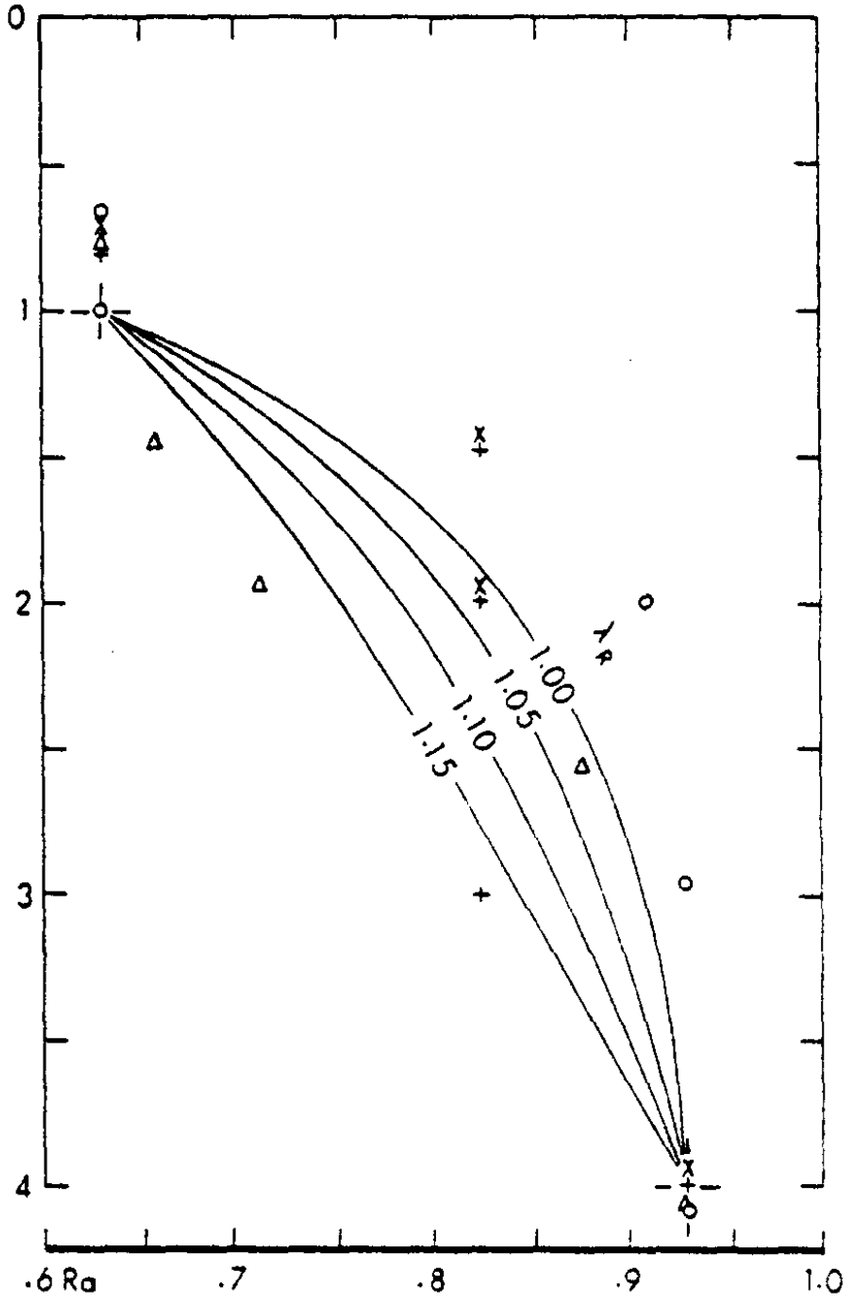

Fig. 6. Radium (in 10^{-13} g/l) as function of depth (km) at four Pacific stations (from MIYAKE and SUGIMURA, 1964). Values have been adjusted to agree at 1 and 4 km. Curves are based on equation (6) for $\gamma = 3{\cdot}3$, and for indicated values of λ_R.

$$w \simeq 1.4 \times 10^{-5} \text{cm s}^{-1}$$

Munk 1966 (Abyssal recipes):

$$\overline{w}\frac{\partial\overline{\rho}}{\partial z} = \kappa_T \frac{\partial^2\overline{\rho}}{\partial z^2}$$

$Q \simeq 25 \times 10^6 \ \frac{m^3}{s} \ (Sv)$ (Deep water formation, radiocarbon data)

$A \simeq 3.6 \times 10^{14} m^2$ (area of oceans) $\longrightarrow$ $w = Q/A \simeq 7 \times 10^{-8} m/s$

For an exponential density profile fitted to observations: $\boxed{\kappa \approx 10^{-4}\ m^2/s}$

Munk and Wunsh 1998 (Abyssal recipes II):

$$\frac{\partial}{\partial z}\left(\overline{w}\,\overline{\rho} - \kappa_T(z)\frac{\partial\overline{\rho}}{\partial z}\right) = \frac{\partial\overline{w}}{\partial z}\rho(z)$$

What powers this mixing?

To relate the turbulent diffusivity (mixing) to energy dissipation:

Assume a production, dissipation balance in the turbulent kinetic energy equation:

$$\overline{\mathbf{u}'w'} \cdot \frac{\partial \overline{\mathbf{u}}}{\partial z} + \overline{b'w'} - \epsilon = 0 \qquad \epsilon = \nu \overline{\frac{\partial u_i}{\partial x_j} \frac{\partial u_i}{\partial x_j}}$$

Then, with $Ri_f \equiv \dfrac{-\overline{b'w'}}{-\overline{\mathbf{u}w} \cdot \frac{\partial \overline{\mathbf{u}}}{\partial z}}$, the flux Richardson number

$$\kappa_T = \frac{-b'w'}{N^2} = \frac{Ri_f}{1 - Ri_f} \frac{\epsilon}{N^2} = \Gamma \frac{\epsilon}{N^2}$$

Where the mixing efficiency is $\Gamma \simeq 0.2$

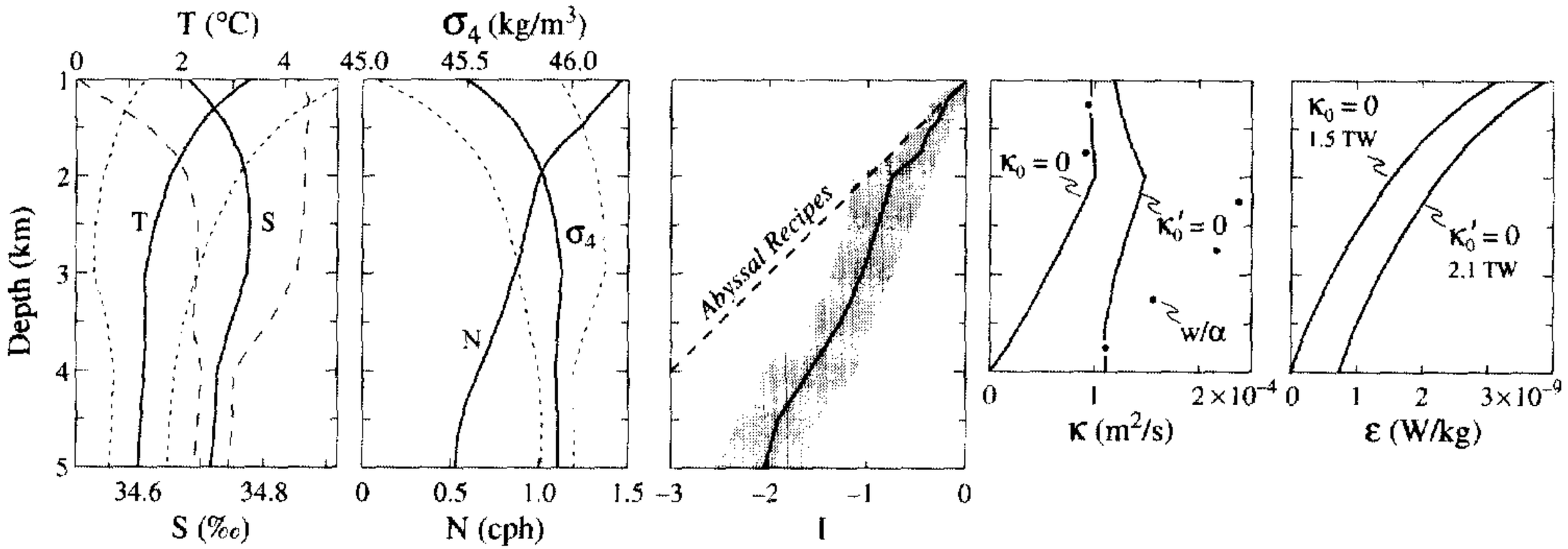

Fig. 2. Procedure for estimating diffusivity $\kappa_{AS}(z)$ and energy dissipation $\varepsilon_{AS}(z)$ required for the maintenance of abyssal stratification. The left two panels show globally averaged profiles of temperature, salinity, density (in σ_4 units), and buoyancy frequency N based on the Levitus Atlas, with error limits as indicated. A lot of scatter occurs in the climatology at depth, and a substantial number of the Levitus profiles are statically unstable (see Jackett and McDougall, 1995). These stations were omitted from the average. The "stratification function" $I(z) = 2\log(N/N_0)$ shown in the third panel (with N_0 taken at 1 km depth) permits the evaluation of $\alpha = dI/dz$. (Abyssal Recipes took a constant α, as shown). The diffusivity $\kappa_{AS}(z)$ and dissipation $\varepsilon(z)$ are derived from $\alpha(z)$ for the two cases $\kappa = 0$ and $\kappa' = 0$ at the lower boundary, under the assumption of a constant $w = 0.7 \times 10^{-7}$ m/s corresponding to 25 Sv of bottom water formation. The global dissipations of 1.3 and 1.9 TW, respectively, are computed from Eq. (3.15) for a mixing ratio $\gamma = 0.2$.

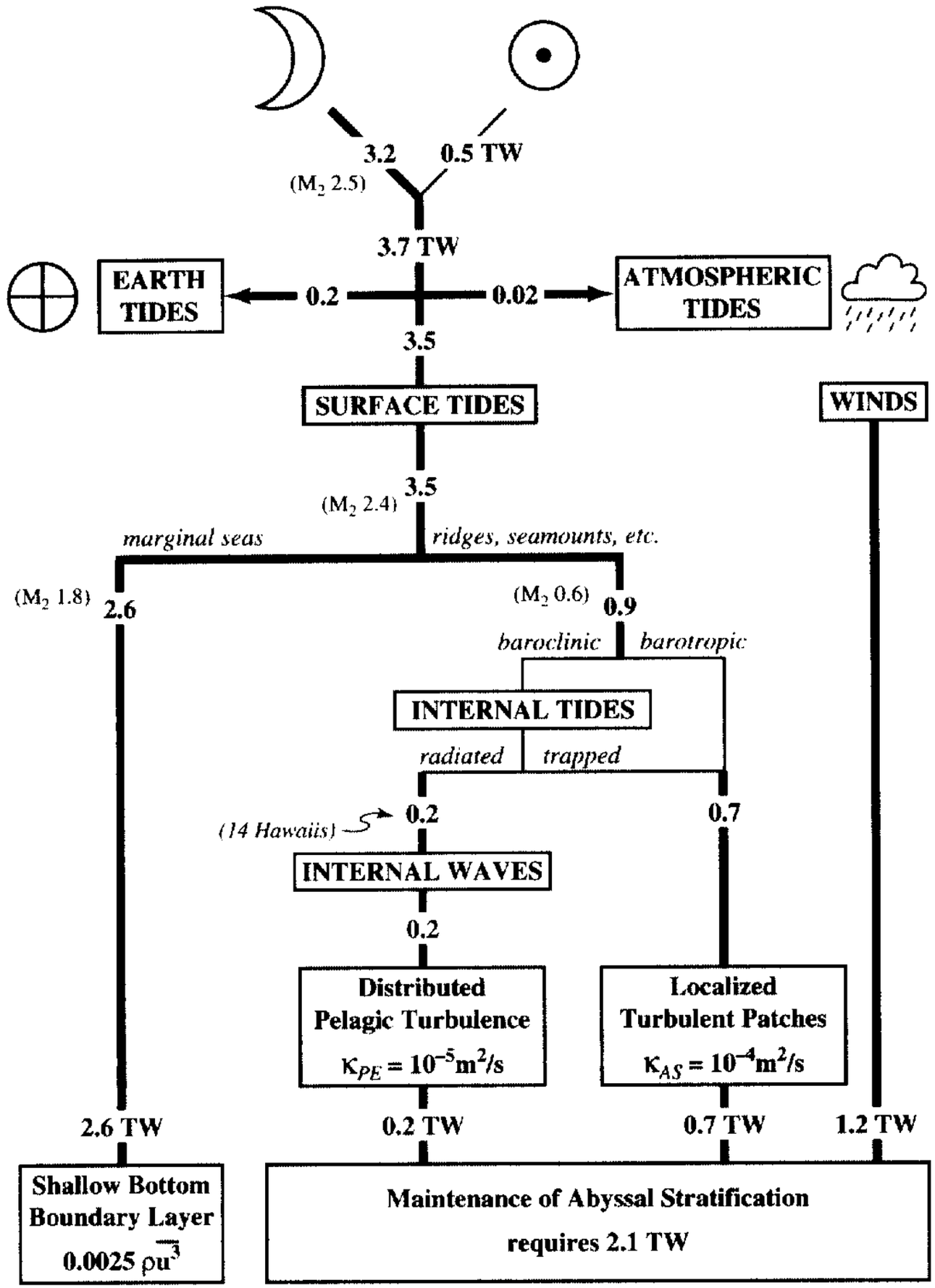
3.2
0.5 TW
(M2 2.5)
3.7 TW
EARTH TIDES
0.2
0.02
ATMOSPHERIC TIDES
3.5
SURFACE TIDES
WINDS
3.5
(M2 2.4)
marginal seas
ridges, seamounts, etc.
(M2 1.8)
2.6
(M2 0.6)
0.9
baroclinic
barotropic
INTERNAL TIDES
radiated
trapped
(14 Hawaiis)
0.2
0.7
INTERNAL WAVES
0.2
Distributed Pelagic Turbulence
κPE = 10−5m2/s
Localized Turbulent Patches
κAS = 10−4m2/s
2.6 TW
0.2 TW
0.7 TW
1.2 TW
Shallow Bottom Boundary Layer
0.0025 ρu3
Maintenance of Abyssal Stratification
requires 2.1 TW

Sandstrom's theorem

A closed steady circulation can only be maintained in the ocean if the heat sources are situated at a lower level than the cold sources (Defant, 1961, page 491).

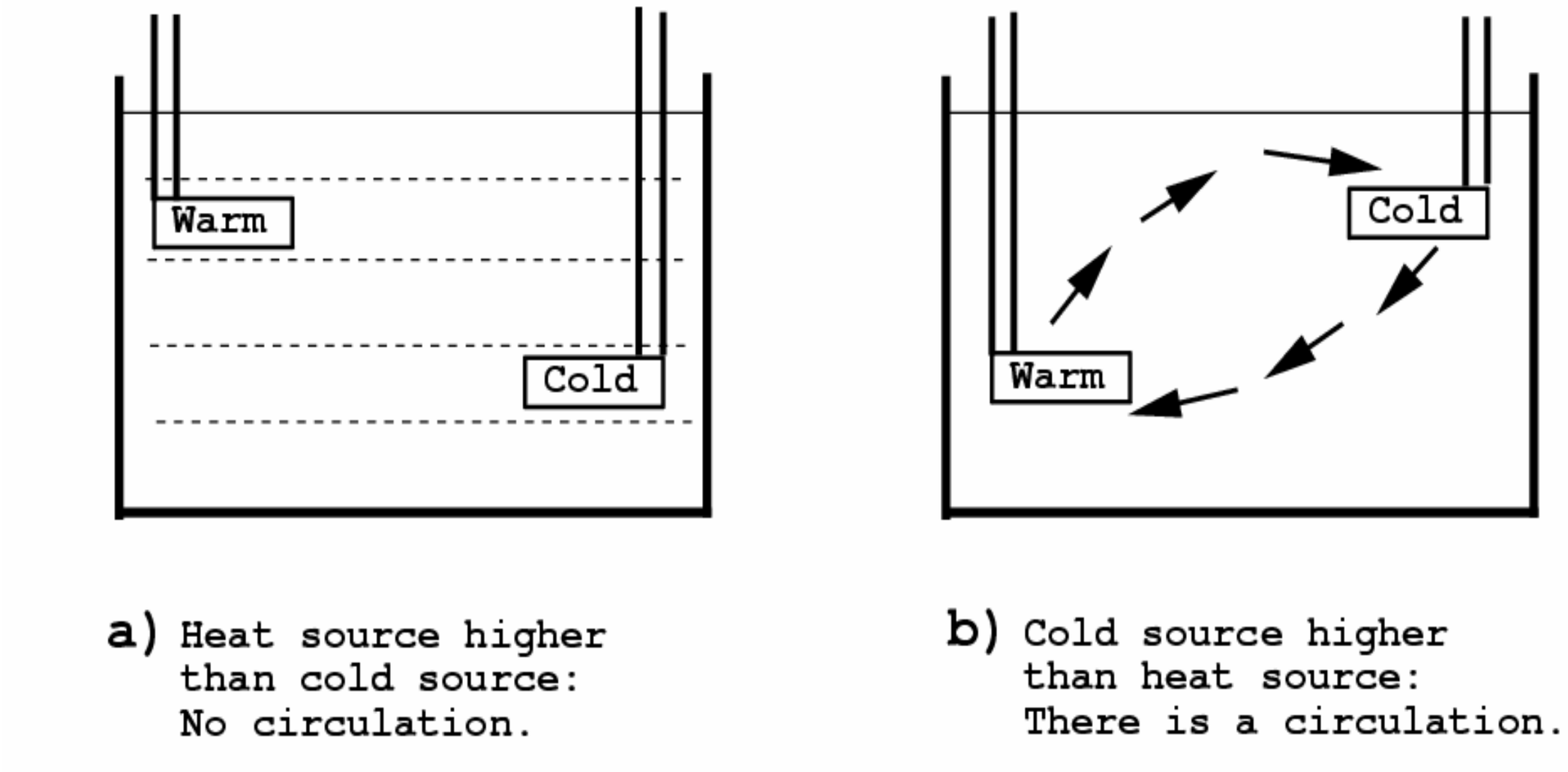

a) Heat source higher than cold source: No circulation.

b) Cold source higher than heat source: There is a circulation.

Microstructure profilers

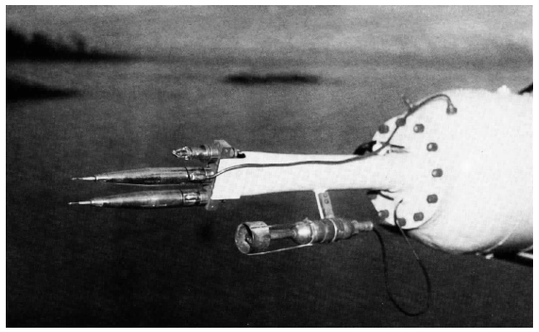

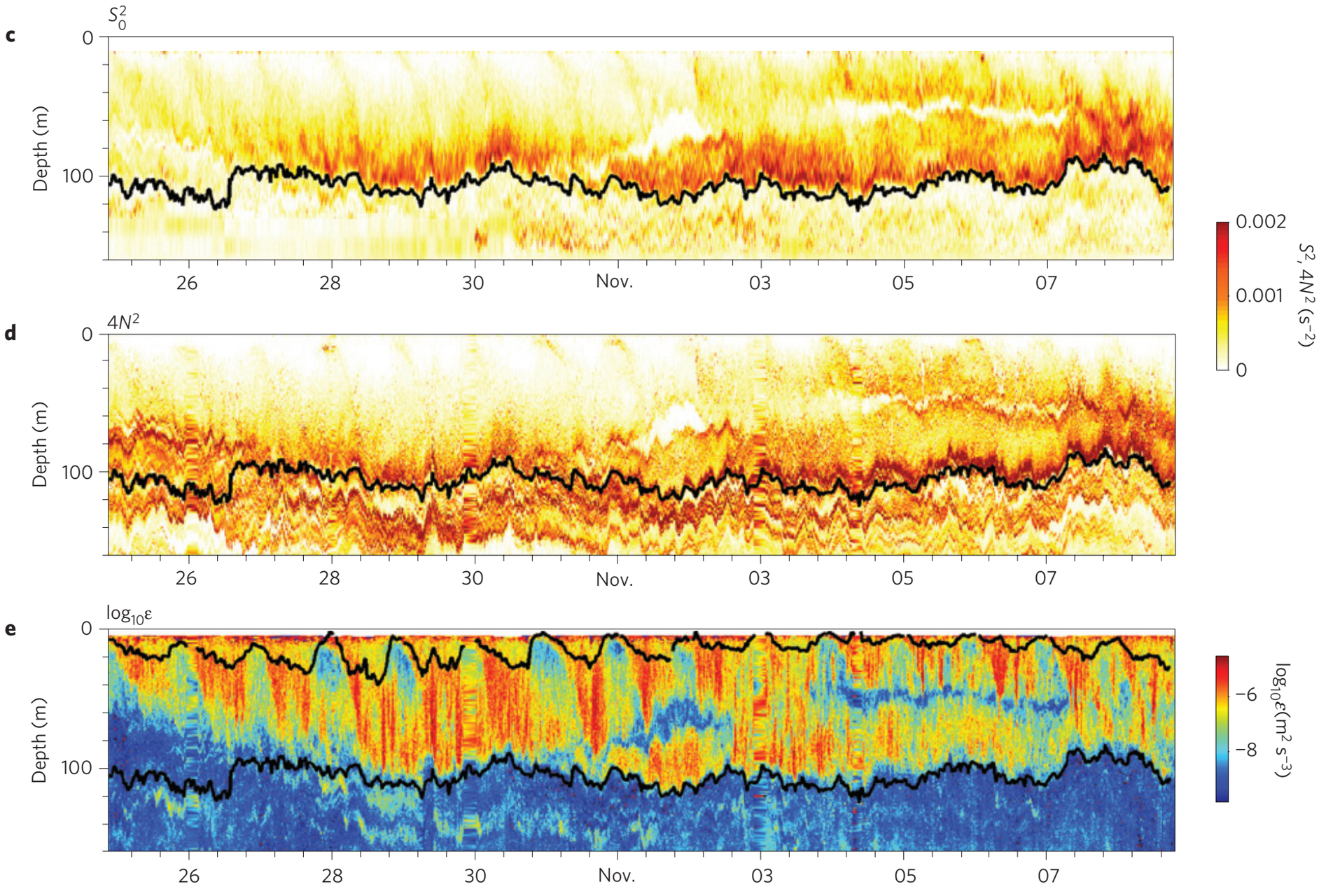

Moum et al. 2009

‘Missing’ Mixing

Problem: Observations of ocean mixing typically find $\kappa \approx 10^{-5}\ m^2/s\ << 10^{-4}\ m^2/s$

Inferred diffusivity, North-South Atlantic section

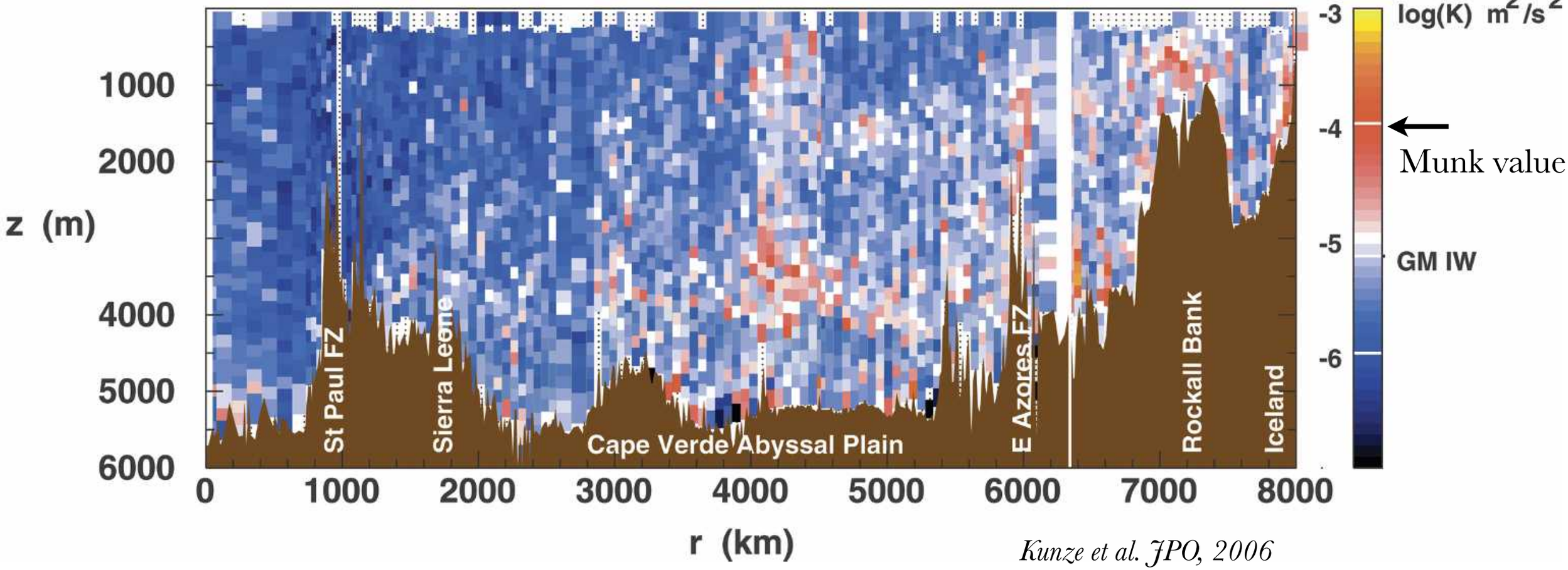

Kunze et al. JPO, 2006

Evidence for slow mixing across the pycnocline from an open-ocean tracer-release experiment

James R. Ledwell*, Andrew J. Watson† & Clifford S. Law†

* Applied Ocean Physics and Engineering, Woods Hole Oceanographic Institution, Woods Hole, Massachusetts 02543, USA
† Plymouth Marine Laboratory, Prospect Place, West Hoe, Plymouth PL1 3DH, UK

THE distributions of heat, salt and trace substances in the ocean thermocline depend on mixing along and across surfaces of equal density (isopycnal and diapycnal mixing, respectively). Measurements of the invasion of anthropogenic tracers, such as bomb tritium and ^{3}He (see, for example, refs 1 and 2), have indicated that isopycnal processes dominate diapycnal mixing, and turbulence measurements have suggested that diapycnal mixing is small[3,4], but it has not been possible to measure accurately the diapycnal diffusivity. Here we report such a measurement, obtained from the vertical dispersal of a patch of the inert compound SF_6 released in the open ocean. The diapycnal diffusivity, averaged over hundreds of kilometres and five months, was 0.11 ± 0.02 cm^2 s^{-1}, confirming previous estimates[1–4]. Such a low diffusivity can support only a rather small diapycnal flux of nitrate into the euphotic zone; it justifies the neglect of diapycnal mixing in dynamic models of the thermocline[25–27], and implies that heat, salt and tracers must penetrate the thermocline mostly by transport along, rather than across, density surfaces.

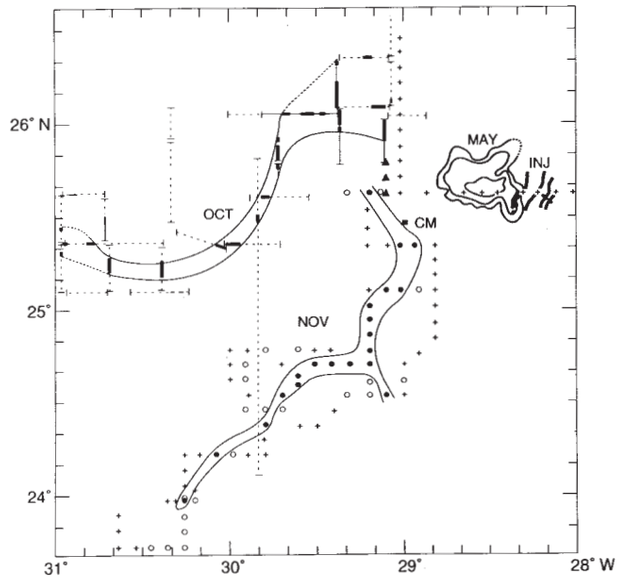

FIG. 1 Evolution of the lateral distribution of the tracer. The injection streaks are shown as short heavy lines near 26° N, 28° W. The contours just to the west show the patch later in May 1992. Heavy lines (further to the west) show tracks for the October survey, where the concentration C at the target surface was >500 fM; light solid lines, C was between 100 and 500 fM; dashed lines, $C \sim 0$. Solid triangles indicate bottle stations occupied at the end of the October cruise, with $C > 300$ fM. Station symbols for the November survey are: plus signs, $C < 30$ fM; open circles, $C = 30$–300 fM; filled circles, $C > 300$ fM. A fine curve has been drawn to envelop the high C regions for the two surveys. CM marks the location of the central mooring for the Subduction experiment.

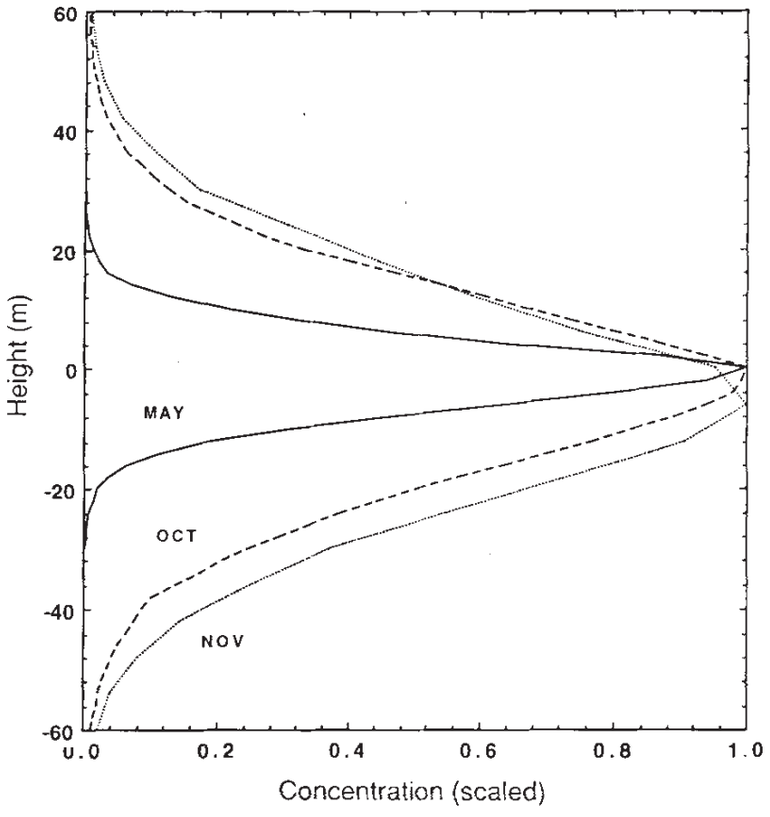

FIG. 2 Evolution of the vertical distribution of the tracer. The mean profiles have been scaled so that the widths can be compared.

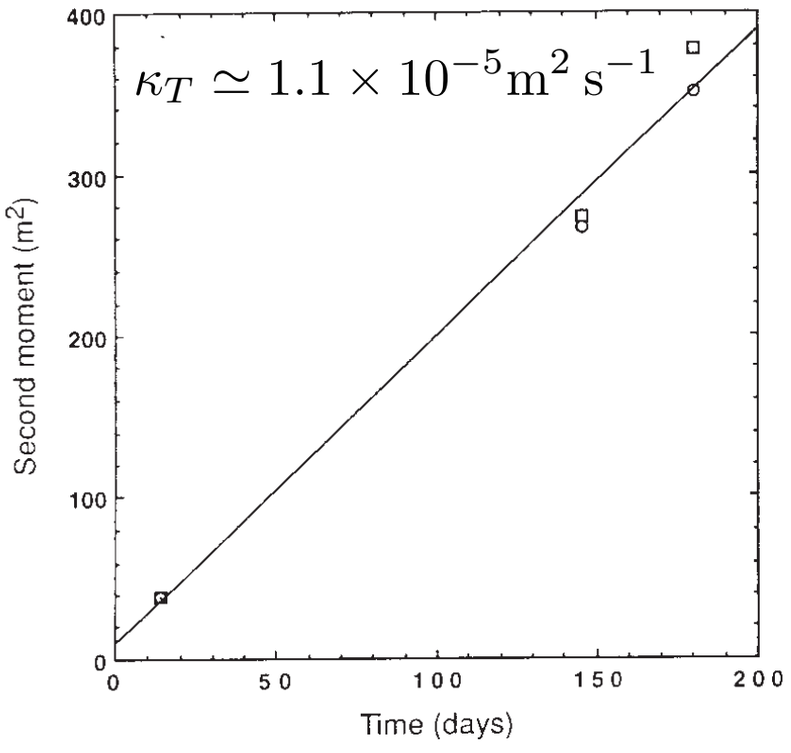

FIG. 3 Growth of the second moment of the vertical tracer distribution. Squares are for raw M_2, circles are for the centre of mass shifted to $h = 0$. The line is for $K_z = 0.11$ cm^2 s^{-1}.

Possible explanations for missing mixing:

- Under-estimate of mixing efficiency
- Boundary mixing
- Horizontal convection
- Upwelling in the Southern Ocean

Mixing Efficiency

Inoue + Smyth 2009

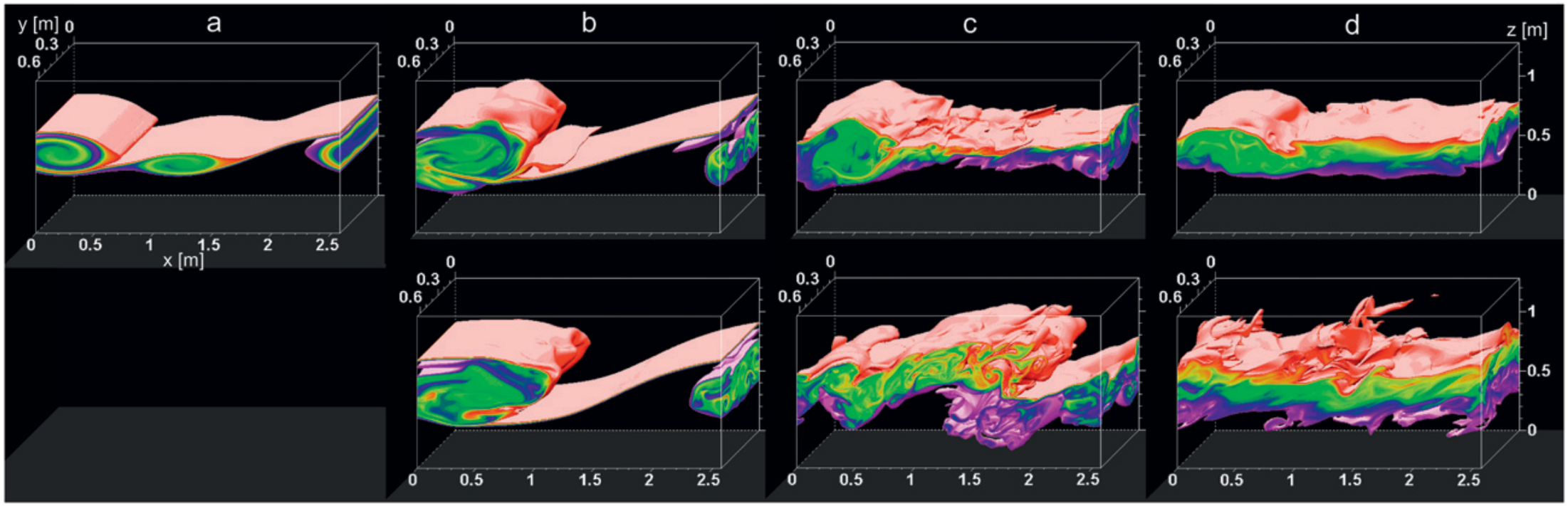

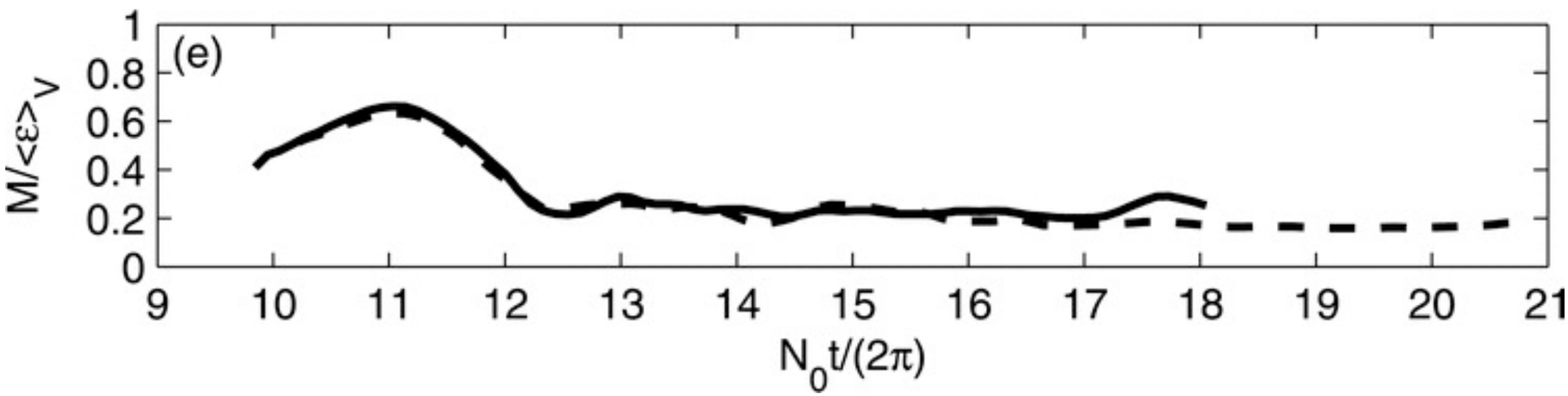

Boundary Mixing

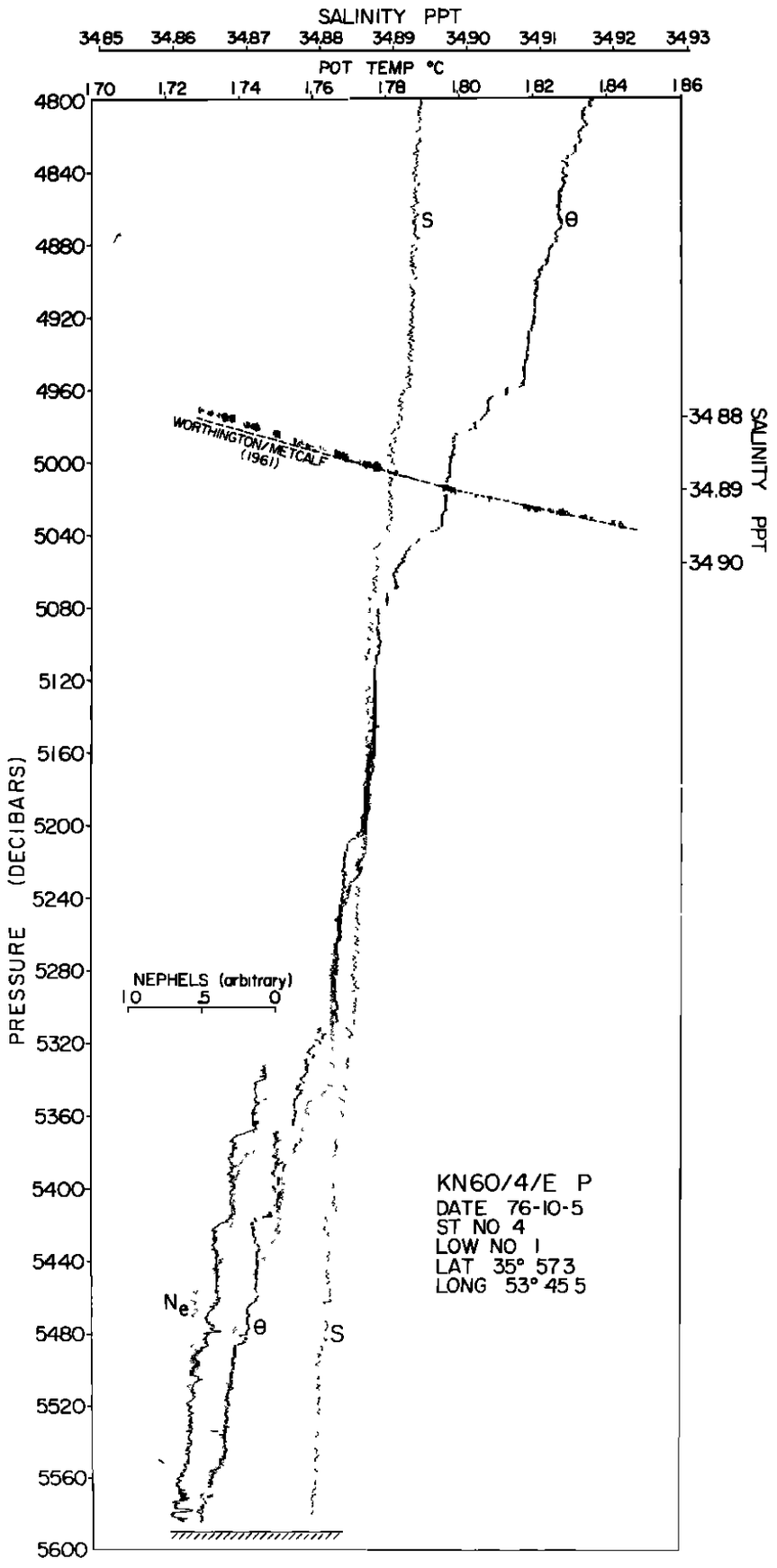

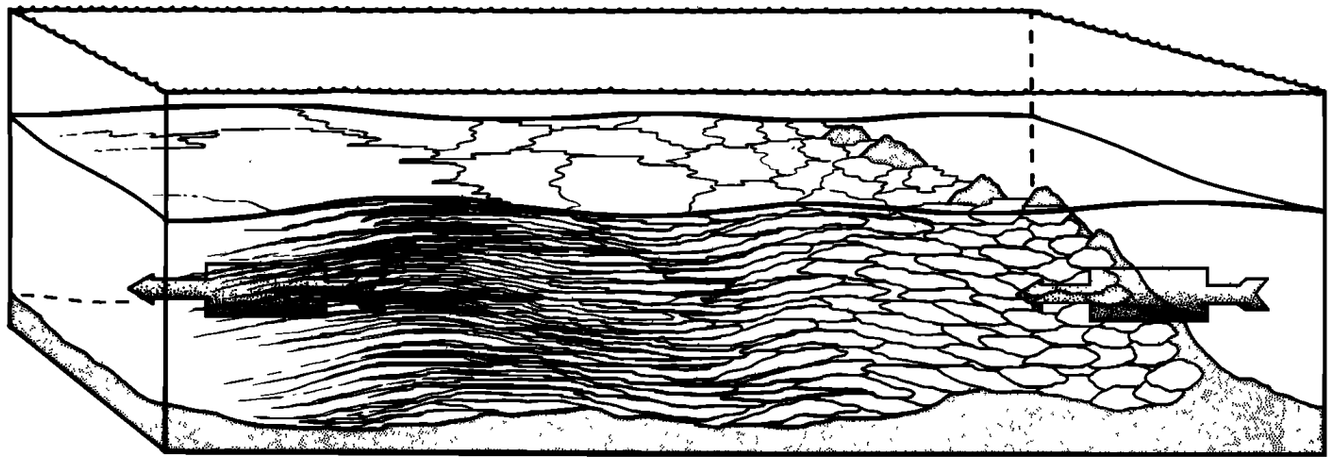

Armi, 1972

Horizontal convection

Hughes and Griffiths 2008

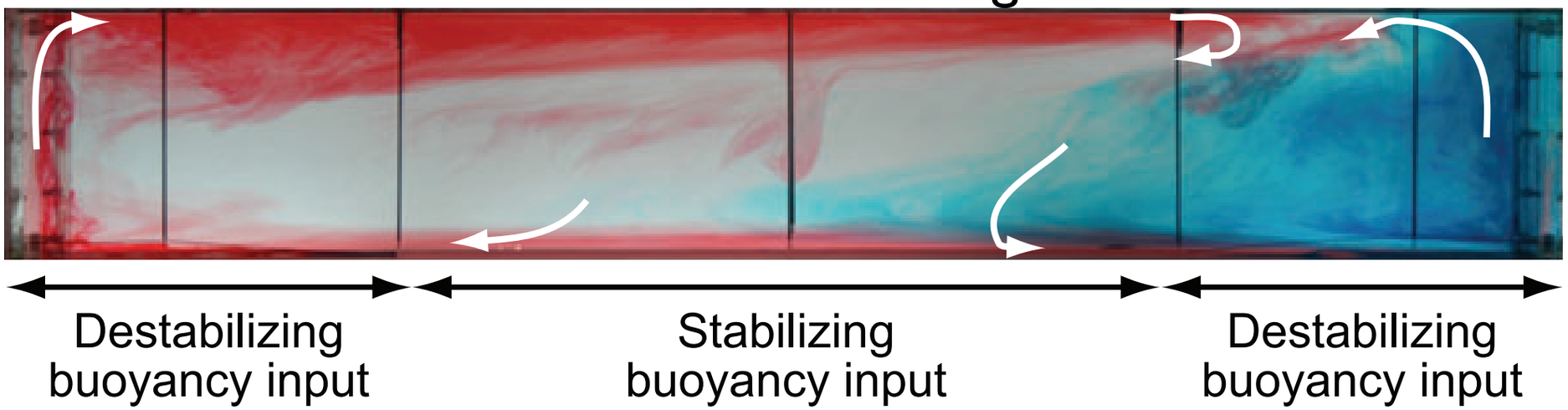

Available Potential Energy and Irreversible Mixing in the Meridional Overturning Circulation

GRAHAM O. HUGHES, ANDREW MCC. HOGG, AND ROSS W. GRIFFITHS

The Australian National University, Canberra, Australia

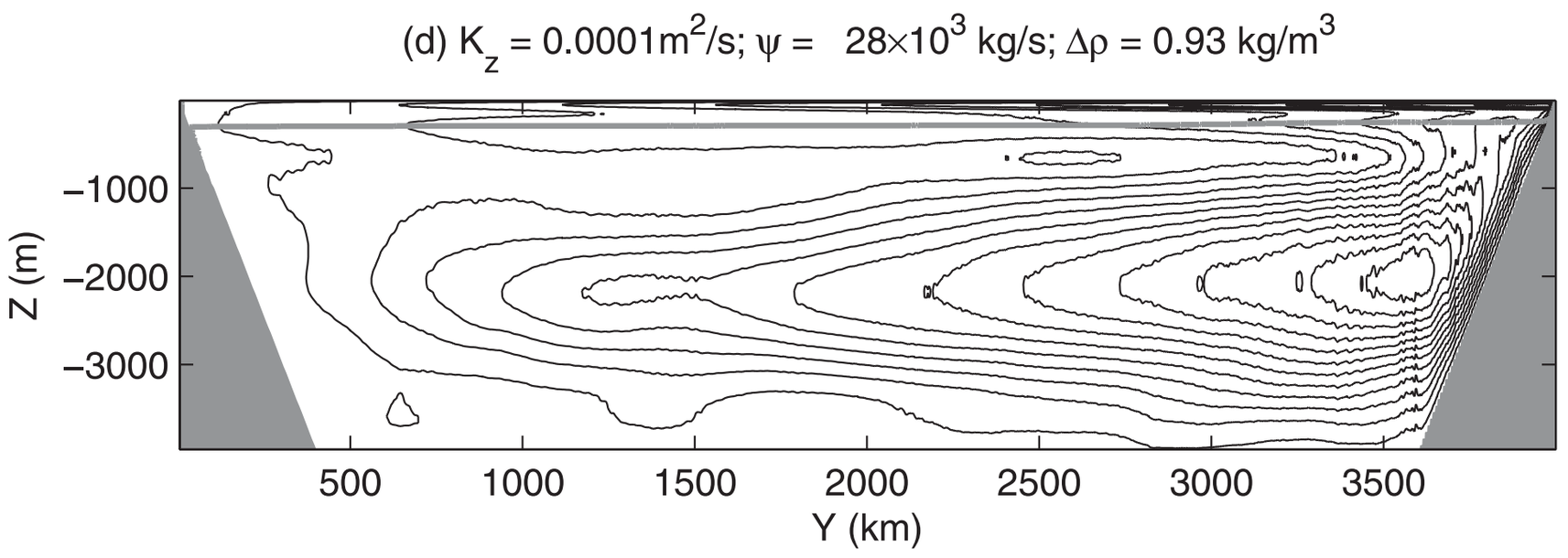

FIG. 4. Dependence of the time-averaged overturning circulation upon the vertical diffusion coefficient (surface buoyancy flux is fixed, with $Q_0 = 200$ W m^{-2}). The maximum streamfunction quoted is that for a two-dimensional flow in a basin of 1-m width, while the density range is $\Delta\rho = \overline{\rho}_{\text{bottom}} - \overline{\rho}_{\text{top}}$. The 20°C isotherm is shown in gray.

Southern Ocean Upwelling

Wunsch and Ferrari, 2004

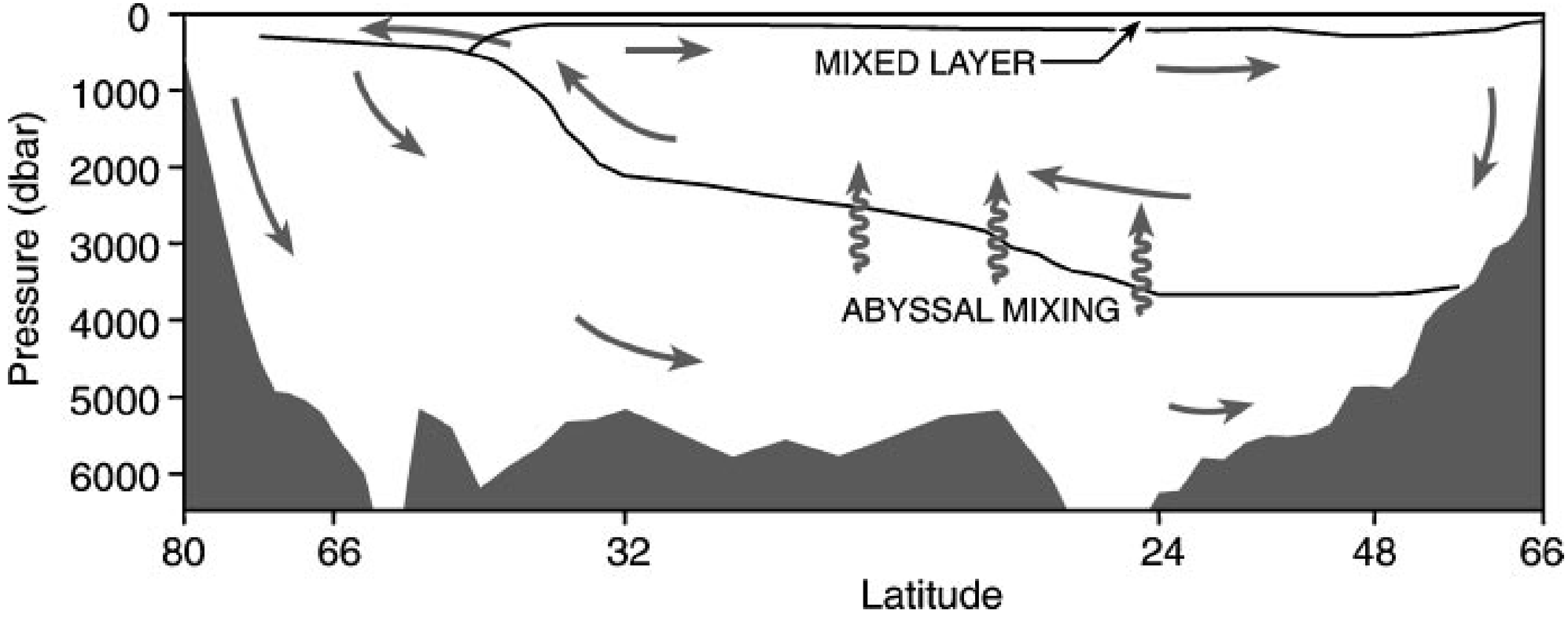

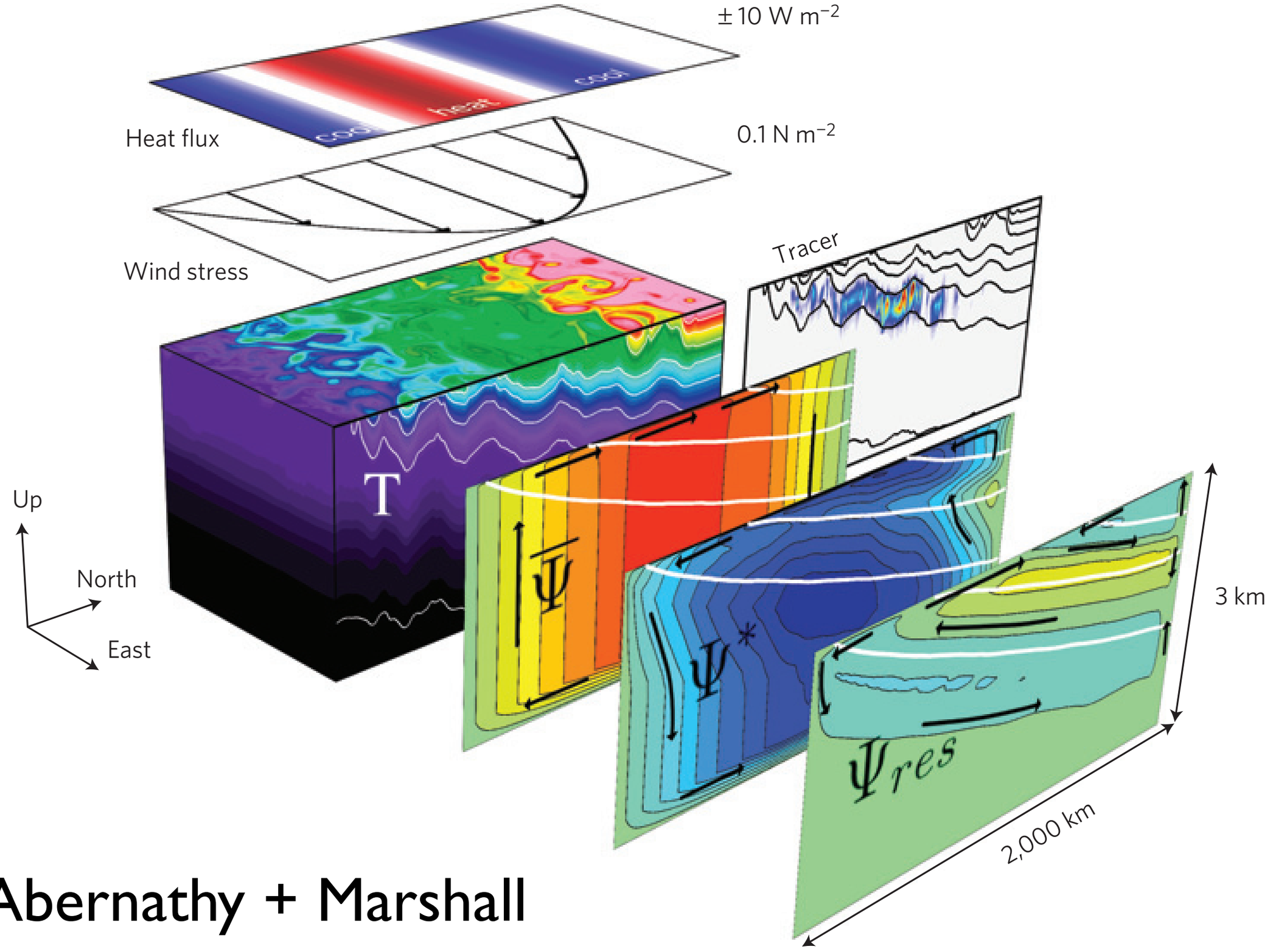

Abernathy + Marshall

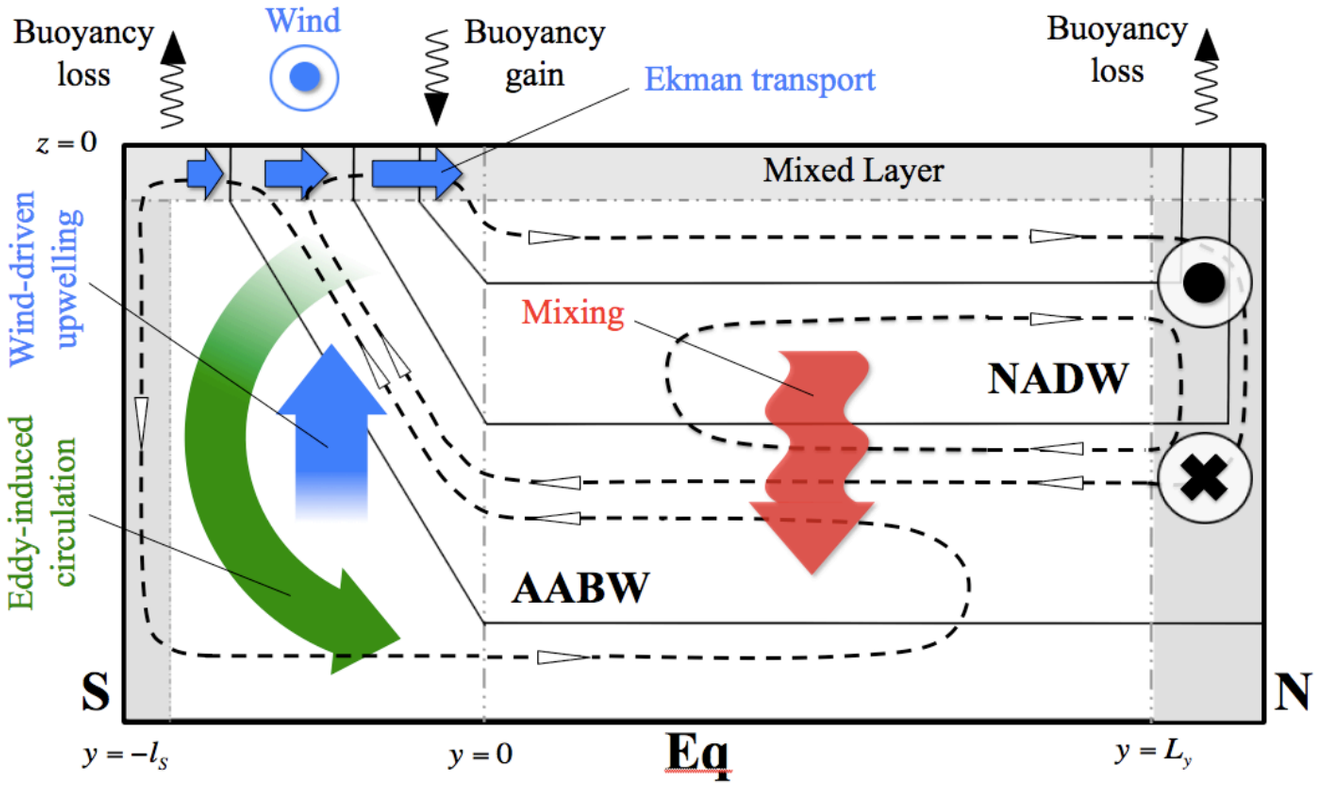

Numerical simulations

$\tau^w = 0.2\ N/m^2 \quad \kappa_v = 2 \times 10^{-5}\ m^2/s$

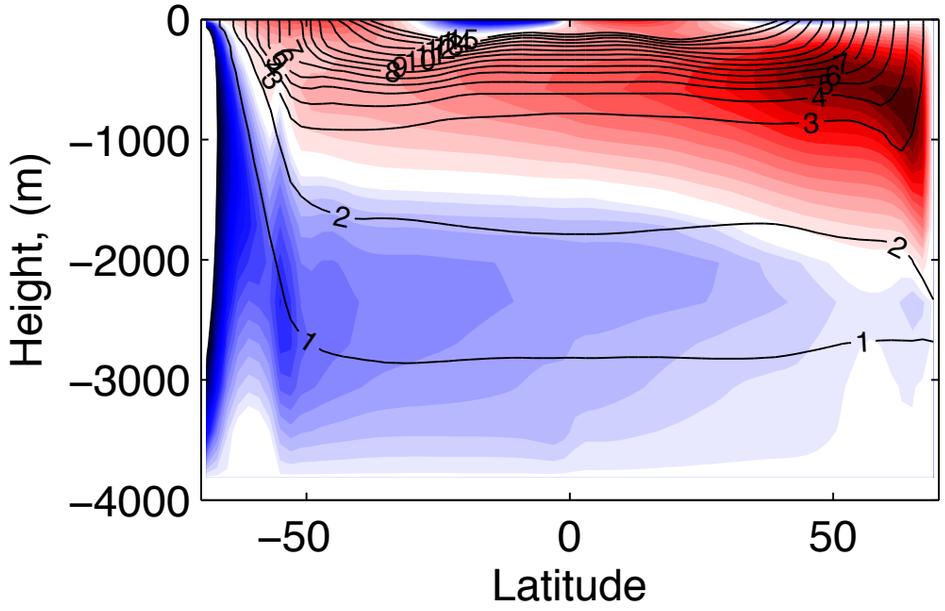

Nikurashin and Vallis, 2011

Course Outline

Intro to Ocean/Atmosphere circulation

1. Motion in a rotating frame
2. Geostrophy
3. Shallow water theory
4. Geostrophic adjustment
5. Inertial waves in a stratified fluid
6. Rossby waves

Large-scale (steady) dynamics

7. Atmospheric circulation
   - 7.1 Westerlies
   - 7.2 Trade winds and the Hadley cell
8. Ocean gyres and Sverdrup flow
   - 8.1 Ekman flow revisited
   - 8.2 Sverdrup flow
9. Western boundary currents
   - 9.1 Stommel-Munk problem

Unsteady dynamics

10. Quasi-geostrophic approximation
    - 10.1 Single layer QG equations
    - 10.2 Waves in QG
    - 10.3 Two-layer equations
11. Baroclinic Instability
    - 11.1 Two-layer Phillips model
    - 11.2 Continuous stratification + Eady model
12. Fronts and frontogenesis
13. Ocean biology
14. Overturning circulation + ocean mixing